Modeling of Electrical Conductivity and Piezoresistivity of Carbon Nanotube Based Polymer Nanocomposites

WEIQING FANG

A THESIS SUBMITTED TO THE FACULTY OF GRADUATE STUDIES

IN PARTIAL FULFILLMENT OF THE REQUIREMENTS

FOR THE DEGREE OF MASTER OF SCIENCE

Graduate Program in

EARTH AND SPACE SCIENCE

York University

Toronto, Ontario

November 2015

Abstract

Superior electrical, thermal, and mechanical properties of carbon nanotubes (CNTs) have made them effective filler for multifunctional polymer nanocomposites (PNCs). In this thesis work, an improved model has been developed to describe the CNT networks inside polymer matrix and thereby evaluated the PNCs' ϕ_c and σ. The new model accounts for the electrical conductance contributed by the continued CNT network across the boundary of adjacent representative volume elements. It more realistically represents the interconnectivity among CNTs and enhances the evaluation of the structure-to-property relationship of PNCs' σ. Furthermore, comprehensive investigations on the piezoresistive behaviour of PNCs have been conducted using developed modeling framework. Quantitative analyses have revealed that piezoresistivity of PNCs is predominantly governed by the three mechanisms related to the strain-induced morphological evolution of the CNT network embedded in the polymer matrix.

Acknowledgement

I would like to give my gratitude to my supervisor, Professor Siu Ning Leung for his generous guidance for my thesis research. Being your first graduate student, it is a great experience to remember.

Special thanks to Yanting Guo, Hao Ding, and the fellow lab members from Multifunctional Materials | Micro-and-Nanostructing Laboratory who kindly provide their help on my works.

Lastly, I would like to dedicate this work to my parents for their great support, motivation and encouragement.

Table of Contents

List of Tables

List of Figures

List of Abbreviations

A = cross-sectional area of the RVE

AFM = atomic force microscope

a = scale parameter of Weibull distribution

b = shape parameter of Weibull distribution

CNT = carbon nanotube

D = diameter of CNT

d = shortest distance between two CNTs

d_{avg} = average CNT-to-CNT distance at junctions

d_{cutoff} = cut-off distance

d_{tunnel} = tunneling characteristic length

d_{vdw} = van der Waals separation distance

e = electron charge

FWHM = full width at half maximum

G_{adj} = electrical conductance with considering the additional conductance contributed by the interconnecting CNTs across the boundary surfaces of the RVE

$G_{boundary}$ = additional electrical conductance in the boundary surfaces of the RVE

G_{RVE} = electrical conductance of the RVE

G_{rect} = electrical conductance of the rectangular cuboid

$G_{RVE,top}$ = electrical conductance of the top RVE

$G_{RVE,bottom}$ = electrical conductance of the bottom RVE

h = Planck's constant

k_B = Boltzmann constant

L = average length of CNT

l = distance between the left and right boundary surfaces of the RVE

l_{avg} = average junction-to-junction distance along a CNT in conductive paths

l_{kl} = distance between two contacting nodes

L_x, L_y, L_z = dimensions of the RVE

M = number of conduction channels of MWNTs

MWNT = multi-walled carbon nanotube

m_e = mass of an electron

N_{CNT} = total number of CNTs in the conductive network

N_{path} = total number of independent conductive paths in the CNT network

$Node_k$, $Node_l$ = contacting nodes

P3OT = Poly(3-octylthiohpene)

PBT = Polybutylene terephthalate

PEO = polyethylene oxide

PET = Polyethylene terephthalate

PNC = polymer nanocomposites

$R_{contact}$ = contact resistance between two CNTs

$R_{contact,avg}$ = average contact resistance at CNT junctions

$R_{intrinsic}$ = intrinsic resistance along an individual CNT

$R_{intrinsic,avg}$ = average intrinsic resistance along a CNT between two junctions

R' = resistance of RVE with applied strain

RVE = representative volume element

SEM = scanning electron microscopy

SWNT = single-walled carbon nanotube

T = respective temperature

t = critical exponent in percolation theory

TEM = transmission electron microscopy

$x_{c,i}$, $y_{c,i}$, $z_{c,i}$ = center point of CNT_i

$x'_{c,i}$, $y'_{c,i}$, $z'_{c,i}$ = center point of CNT_i with applied strain

$x_{i,1}$, $y_{i,1}$, $z_{i,1}$ = starting point of CNT_i

$x_{i,2}$, $y_{i,2}$, $z_{i,2}$ = ending point of CNT_i

α = strain ratio of CNT to polymer

σ = electrical conductivity

σ_0 = physical parameter in percolation theory

σ_{adj} = electrical conductivity after accounting for the contribution of the interconnecting CNTs across the boundary surfaces of the RVE

σ_{CNT} = intrinsic electrical conductivity

σ'_{CNT} = intrinsic electrical conductivity with applied strain

T = transimission probability

θ_{avg} = average polar angle of CNTs

θ_i = polar angle of CNT_i

θ'_i = polar angle of CNT_i with applied strain

θ_{max} = maximum alignment angle of CNT

ϕ = volume fraction of the fillers

ϕ_c = percolation threshold

φ_i = azimuthal angle of CNT_i

φ'_i = azimuthal angle of CNT_i with applied strain

ε_{poly} = applied strain

υ = Poisson's ratio of PNC

ΔE = height of the potential barrier

ΔR = change in the resistance of RVE with applied strain

CHAPTER 1 Introduction

1.1 Electrical conductivity and piezoresistivity of PNCs

Various nano-scale carbon fillers, such as carbon nanotubes (CNTs), are promising for superior mechanical (Dalton 2003, Shtogun 2010), electrical (Ebbesen 1996), and thermal (Hou 2006) properties. Such relatively new class of fillers has led to great potential in fabricating multifunctional polymer nanocomposites (PNCs), which are considered as realistic alternatives to conventional smart materials in photogating transistor (Marcus 2006), electron field emission (Matsubara 2008), magnetic nanomaterials (Glenis 2010), and resistance-type strain sensors of high sensitivity (Alamusi 2011). Especially in the field of resistance-type strain sensor, it was guaranteed that integrating nano-scale carbon fillers into polymers would open up great opportunities in fabrication of PNCs with tailored piezoresistivity (i.e., the strain-induced change in resistance). Due to its outstanding static and low-frequency dynamic responses, this type of strain sensors, based on piezoresistive PNCs, has great potential for its implementation on structural health monitoring, wearable sensor, impact events monitoring, and delamination in laminates.

The distinguished mechanical and intrinsic electrical properties of CNTs make them the ideal reinforcing agents for the fabrication of multifunctional PNCs. It is possible to embed only a small amount of CNTs in a polymer matrix to achieve significant enhancement in the electrical conductivity (σ), due to the exceptionally high intrinsic electrical conductivity and extremely high aspect ratio of CNTs. Meanwhile, small filler loadings also allow PNCs to maintain the favorable properties of polymers, including low density, high

chemical resistance, and good processability. Based on the percolation theory (Kirkpatrick 1973), there exists a critical concentration of conductive fillers, namely percolation threshold (ϕ_c), over which further increase in filler loading would generate a conductive percolation network and make the PNCs to transit from electrical insulator to conductor. Once the filler contents achieved percolation threshold, the electrical conductivity of PNCs will be enhanced by several orders of magnitude.

Experimental studies have been conducted by many researchers to explore the effects of various morphological factors of CNT network (i.e., dispersion, alignment, and aspect ratio) on PNCs' electrical properties. Meanwhile, theoretical and numerical works have been performed to investigate the morphology-property relations. Researchers have performed Monte Carlo simulation to model the conductive network inside PNCs. The 2D, multi-2D layers, or 3D random resistor network can be generated in finite-size representative volume elements (RVEs). Such RVEs was assumed to be periodically repeated to represent the PNCs. In earlier simulation work (Hu 2008a). Generally, RVEs is chosen as a cube, where electric current will propagate along the conductive path generated by CNTs from one boundary surface to the opposite surface. The periodic configuration of CNTs is considered in their work such that the portion of CNTs, which extended outside the boundary surface, was relocated into the cube, pointing into the cell from the opposite boundary surface. However, this method discounted the CNTs' interconnectivity through the boundary surface, and thereby their contribution to the RVE's effective conductance. A sufficiently large representative cell and high computation cost were required to obtain accurate simulation results, such that the error caused by the ignorance of these continuous CNTs would reduce.

Thus, an advanced model is required to obtain more realistic results and to promote the calculation efficiency.

PNCs with improved electrical conductivity can further be modified for applications as highly sensitive strain sensors, due to their strain-induced resistivity change (Alamusi 2011). In recent experimental studies, linear relationship between the applied external strain and the relative change in PNC specimen's resistance were observed. It is revealed that the piezoresistive behaviour of PNCs was qualitatively attributed to following mechanisms: (i) reconfiguration of CNTs conductive network in the PNC; (ii) change in tunneling resistance at CNTs junctions; and (iii) change in the intrinsic electrical resistance of CNTs. However, fundamental understanding and quantitatively systematical analysis of the mechanisms contributed to the piezoresistive behaviours in PNCs filled with CNTs have yet been elucidated. Thus, a new model is required to realistically simulate the strain-induced morphology evolution of the conductive network and the resultant macroscopic piezoresistive behaviours of PNCs. Such model can help to reveal the underlying mechanism of PNCs' piezoresistive behaviours and derive the structure-to-property relationship.

In this thesis research, a new random resistor network model in 3D dimension has been developed to simulate the electrical conductivity of the PNCs. In this new model, the interconnectivity of those CNTs crossing the boundary surfaces of the representative volume element is considered. This would lead to more accurate simulation results while maintaining high calculation efficiency. Systematically and quantitative investigation of the governing factors of PNC's electrical conductivity were performed using the developed model. Subsequently, the new model has been extended to simulate the piezoresistivity (i.e.,

strain-induced relative change in resistance) of PNCs filled with CNTs. The strain-induced evolution in conductive network has been realistically simulated in the improved model. Consequently, the underlying mechanisms of the piezoresistivity have been discovered.

1.2 Thesis objectives

The long-term goal of the research is to develop polymer nanocomposites with tailored electrical and piezoresistive properties, and eventually for thermal energy harvesting application. During the course of my Master's studies, the thesis research aims to investigate the morphology-property relationship and develop a new approach to elucidate the governing factors of these properties in PNCs. In this thesis, an improved 3D random resister network model has been developed to theoretically study the effects on electrical and piezoresistive properties of PNCs.

1.3 Thesis organization

The main body of this thesis consists of five chapters. The extensive and systematical literature review is presented in Chapter 2 *Background and Literature Review*. Chapter 3 *Electrical Conductivity of PNCs* reports the development of a new model that describes the electrically conductive CNT network in a polymer matrix, and subsequently the uses of this model to numerically study the structure-to-property relationship in CNT-polymer nanocomposites. In Chapter 4 *Piezoresistivity of PNCs*, the modeling work of piezoresistivity is presented. It also reports quantitative investigations on the governing factors of PNC's piezoresistive behaviours. Chapter 5 provides the concluding remarks of the thesis research.

CHAPTER 2 Background and Literature Review

2.1 Electrical conductivity of PNCs

Recently, great attention has been paid to the fabrication of electrically conductive polymer nanocomposites (PNCs) with the use of various conductive fillers. In particular, carbon nanotubes (CNTs), including single-walled carbon nanotubes (SWNTs) and multi-walled carbon nanotubes (MWNTs), are considered to be powerful and effective fillers for enhancing the electrical conductivity of PNCs. In recent decade, experimental and numerical studies on the electrical conductivity of nanocomposites made from insulating polymers filled by CNTs have been carried out. This section describes the percolation phenomena, which represents the insulator-to-conductor transition, of PNCs. Moreover, the recent modeling schemes for PNCs' electrical conductivity; the recent studies on the effects of intrinsic conductivity of CNTs, tunneling of contacting CNTs, distribution of CNT length, and degree of CNT alignment are systematically reviewed.

2.1.1 Percolation phenomenon of electrically conductive PNCs

Due to the exceptional electrical properties and extremely high aspect ratio of CNTs, it is possible to embed only a small amount of CNTs in polymer matrix to achieve significant enhancement in the electrical conductivity of PNCs (Dalton 2003). Generally, by gradually increasing the loading of the conductive fillers (e.g, CNTs) inside the insulating polymer matrix, the evolution of the conductive network, the percolating phenomenon, has been divided into three stages by Alamusi et al. (Alamusi 2011). As shown in Figure 2.1, in the first stage (i.e., state "I"), the electrical conductivity of PNCs is close to that of the neat polymer, since the amount of CNTs is not sufficient to generate a conductive path inside the polymer

matrices, as shown in Figure 2.2(a). As the CNT loading increased, some large clusters connected by CNTs are gradually formed, which meant that the tunneling effects among these neighboring CNTs become more significant. The electrical conductivity of composites increases gradually, though the conductive path is not well established by CNTs. In the second stage, state "II" in Figure 2.1, a preliminary conductive path is completed, as the highlighted path in Figure 2.2(b). The electrical conductivity of PNCs increased dramatically, since the critical concentration of CNTs, namely percolation threshold, is reached. Consequently, the PNC transited from electrical insulator to conductor due to its electrical conductivity has been enhanced by several orders of magnitude. In the final stage, state "III" in Figure 2.1, with further addition of CNTs into polymer matrices, the electrical conductivity increased gradually. At this stage, the electrically conductive network within a lot of paths is well established inside polymer matrices, as shown in Figure 2.2(c). Based on such percolating phenomenon, Kirkpatrick developed the percolation theory to describe such dependence of PNCs' electrical properties on CNT loading (Kirkpatrick 1973). The theory can be mathematically represented by Equation (2.1).

$$\sigma = \sigma_0(\phi - \phi_c)^t \text{ for } \phi > \phi_c \qquad (2.1)$$

where σ_0 is a physical parameter commonly attributed to the intrinsic conductivity of CNTs; t is the critical exponent, which is known to be dominated by the dimensionality of the system; ϕ is the volume fraction of the fillers; and ϕ_c is known as the percolation threshold.

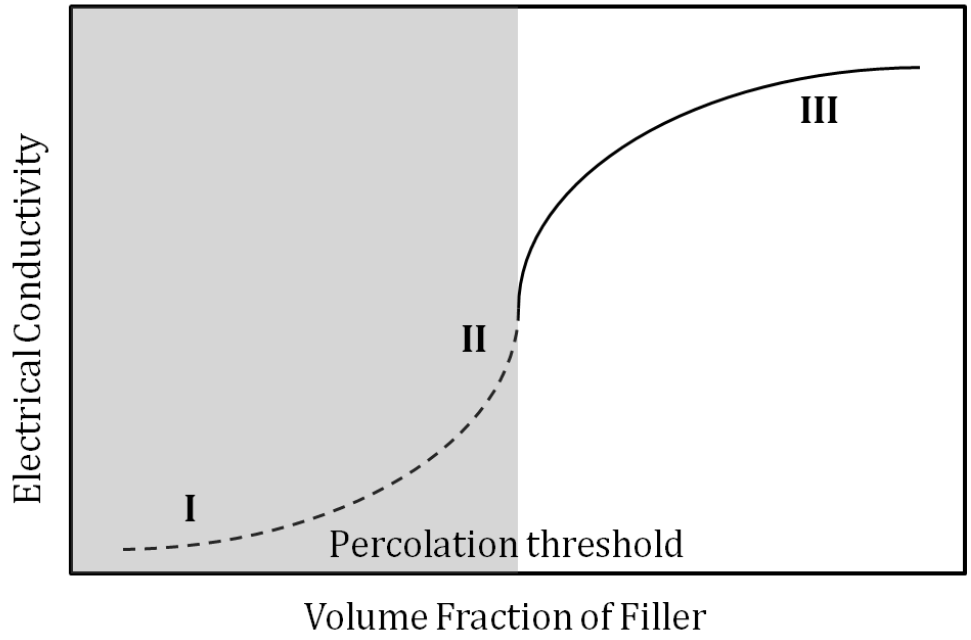

Figure 2.1 Electrical conductivity of PNCs at varying filler loading, where "I, II, and III" denote the different states as PNCs transiting form insulator to conductor.

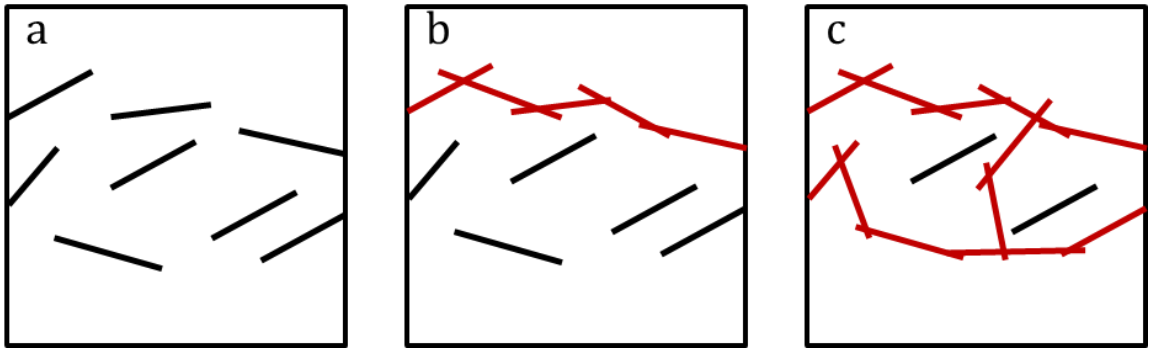

Figure 2.2 Schematics of the percolation process in PNCs (i.e., the formation of conductive paths in polymer matrices).

The aforementioned percolation phenomenon was demonstrated in many previously published experimental results using various types of CNTs, such as SWNTs and MWNTs. The electrical conductivity of SWNT/Poly(3-octylthiohpene) (P3OT) was investigated by

Kymakis *et al.* (Kymakis 2002). The reported percolation threshold was around 11 wt.%. In their study, the doping of a polymer (i.e., P3OT) with SWNTs formed a conductive composite and thereby increased the electrical conductivity by five orders of magnitude. Lower percolation threshold, 4 wt.%, was achieved in their later work (Kymakis 2006) using purified SWNTs. Nogales et al. reported that the preparation of SWNT/Polybutylene terephthalate (PBT) nanocomposites using *in situ* polycondenstaion led to much lower percolation threshold (Nogales 2004). It was revealed that the intense dispersion process by ultra-sonication and ultrahigh-speed stirring of SWNTs in PBT and the subsequent *in situ* polycondensation process significantly decreased the percolation threshold. For MWNTs, Hu et al. fabricated MWNT/Polyethylene terephthalate (PET) nanocomposites using coagulation process (Hu 2006). Transmission electron microscopy (TEM) and scanning electron microscopy (SEM) were used to confirm the uniform dispersion of MWNTs throughout polymer matrix.

2.1.2 Modeling electrical conductivity of PNCs.

In the Monte-Carlo simulation that determines the macroscopic electrical conductivity of PNCs using a microscopic representative volume element (RVE), it is assumed that CNT are uniformly dispersed in polymer matrices. Generally in the 3D modeling, a 3D resistor network model would be constructed inside a RVE to predict the macroscopic electrical conductivity of nanocomposites (Alamusi 2011). In previous works (Bao 2011, Hu 2008a), the RVE was assumed to be periodically repeated to represent the macroscopic behaviours of the PNC, due to the aforementioned uniform distribution of CNTs inside the polymer matrices. The individual CNT was represented as a "soft-core" capped

cylinder with length of *L* and diameter of *D* shown in Figure 2.3. The highlighted dash line is its axle. Such CNTs were randomly distributed in the RVE where periodic boundary conditions were adopted for CNT configurations. Hu et al. considered the CNTs extruding through the RVE's boundary surface to be part of the adjacent RVE by cutting the extruding portion and relocating it onto the opposite boundary surface (Hu 2008a). However, such approach overlooked the interconnectivity of CNTs across the boundary surface. Thus, it required a RVE of large volume, where the boundary condition was negligible, in order to achieve numerical convergence. Although the large RVE will significantly increase the computation cost (i.e., running time and memory), a RVE that was sufficiently large (i.e., the dimension of the cuboid RVEs were chosen as five times the length of CNTs) were chosen in their numerical work. Bao et al. developed a modeling scheme by considering periodically connective paths on opposite surfaces of the RVE. It permitted the simulations using a relatively small RVE. Nevertheless, there were still some possible cases of interconnecting CNTs across the boundary surfaces of adjacent RVEs that were disregarded under this approach (Bao 2011). In their work, converged simulation results using RVE with various sizes were obtained at high CNT loading (i.e., >1.0 vol.%). However, the difference in the simulation results using various RVE at low CNT loading (i.e., <1.0 vol.%) was obvious. Furthermore, the "cut-and-relocate" approach, which adopted in both studies to handle CNTs extruding out of the RVE, would lead to immediate decrease in the length of those cut CNTs, and thereby generated unnecessary bias on the length distribution of CNTs.

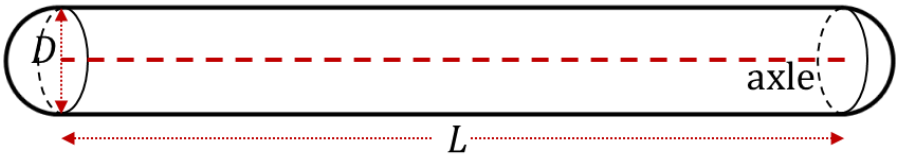

Figure 2.3 3D representative element of CNT (i.e., "soft-core" capped cylinder) with length of *L* and diameter of *D*.

In general, if considering the sites inside the RVE occupied by CNTs as conductors with electrical conductivity equals to the intrinsic conductivity of CNTs and the sites not occupied by CNTs as insulators with electrical conductivity equals to zero, the determination of the PNCs' electrical conductivity requires the identification of the interconnectivity among CNTs. In the numerical work by Hu et al., the shortest distance *d* (i.e., the length of the common perpendicular to axial lines of CNTs) between two CNTs were determined. If *d* was smaller than the diameter of the CNTs, the two CNTs were identified as in the state of contact (Hu 2008a). In this numerical work, the contact resistances were ignored. In the later work by Bao et al., the contact resistances, which were caused by the electron ballistic tunneling through the contact junction between two CNTs, were considered in generation of conductive network (Bao 2011). The formulas used in the calculation of contact resistance will be discussed in detail in later section. Thus, two types of resistances in such conductive network were considered, namely the intrinsic resistance along CNTs and contact resistance between two interacting CNTs. After identifying the percolating conductive network of CNTs inside RVE as well as calculating the two types of resistances, Kirchhoff's circuit laws were applied to calculate the effective electrical conductivity of the percolating network. In both of the 3D modeling works by Hu et al. and Bao et al., Monte Carlo simulation scheme was

applied to obtain a converged average value of simulated conductivity which represented the macroscopic electrical conductivity of PNCs.

2.1.3 Intrinsic conductivity of CNTs

Compact physical model was developed for the intrinsic conductivity of CNTs by Naeemi et al. (Naeemi 2009). In their work, they investigated the conduction mechanism of SWNTs and MWNTs. The relationship between intrinsic conductivity of CNTs and their dimensions (i.e., length and diameter) were systematically revealed.

Diameters of CNTs, in particular MWNTs, may vary from few nanometers to hundreds of nanometers. Meanwhile, their number of shells may vary from a few to many. Initially, most experiments indicated that only the outer shell in a MWNT conducts. Recently, however, it has been confirmed that all shell are also contributive to electrical conductivity (Li 2005). In the numerical work by Naeemi et al., they assumed that the shells have random chirality, and statistically one third of the shells were going to be metallic while the rest are semiconducting (Naeemi 2009). Based on this concept, Naeemi et al. systematically investigated the linear dependence of average number of channels per shell on shells diameters. Furthermore, the intrinsic conductivity of MWNTs with various diameters was studied systematically in their work. The intrinsic conductivity with different dimensions (i.e., diameter and length) can be extracted from the plots of electrical conductivity of MWNTs with various diameter and length.

2.1.4 Tunneling effect of two contacting CNTs

For the dispersion of CNTs in a polymer matrix, due to the high surface-to-mass ratio of CNTs, molecular scale forces and interactions should be considered among CNTs. Specifically, van der Waals forces usually promote flocculation of CNTs, whilst electrostatic charges or steric effects lead to a stabilization of the dispersion through repulsive forces (Hu 2006). In the work by Hu et al., it was reported that CNTs dispersed inside polymer matrices were coated or encapsulated with a thin insulating polymer layer, due to the interaction between CNTs and the polymer. The contact region between two CNTs was at the nano-scale, the dimension of which would be less than the momentum relaxation length and Fermi wavelength (Venema 1999, Rubio 1999). In the work by Bao et al., the electron tunneling through the contact junction was reported in the ballistic transport range (Bao 2014), which can be described in Equation 2.2.

$$R_{contact} = \frac{V}{I} = \frac{h}{2e^2} \cdot \frac{1}{M\mathrm{T}\left[1 + \frac{\pi^2}{6}\left(\frac{k_B T}{\Delta E}\right)^2 \ln \mathrm{T}\,(\ln \mathrm{T} + 1)\right]} \qquad (2.2)$$

where h is Planck's constant, e is electron charge, M is the number of conduction channels, T is transimission probability for the electron to tunnel through the polymer obstacle between CNTs, k_B is Boltzmann constant, T is the respective temperature, and ΔE is the height of the potential barrier which is the difference of the work functions between the CNT (Shiraishi 2011) and polymer (Davis 1969). At room temperature (i.e., T = 300K), the temperature effect on $R_{contact}$ can be ignored, since $k_B T$ = 0.026 eV is much smaller than ΔE = 1~5 eV (Li 2007, Hu 2008b). Thus, the formula can be adopted as Equation 2.3.

$$R_{contact} = \frac{V}{I} = \frac{h}{2e^2} \cdot \frac{1}{M\mathrm{T}} \tag{2.3}$$

The tunneling effect contributes significantly to the conductive network of CNTs, especially around the percolation threshold. Thus, it is necessary that the resistances due to the tunneling effect of two contacting CNTs are considered in 3D modeling for electrical conductivity of PNCs along with intrinsic conductivity of CNTs as described in the previous section.

2.1.5 Characterization of CNT length distribution

For molecular particles, the physicochemical properties such as molecular weight, chemical composition, purity, solubility, and stability are usually necessary to analyze. These properties can be investigated using some well-established techniques, such as gas chromatography, infrared spectroscopy, nuclear magnetic resonance, mass spectrometry, and ultraviolet-visible spectroscopy. However, for CNTs dispersing in polymer matrices, it is challenging to characterize these properties (i.e., the length of CNTs). Experimental evidence on the effect of CNT length on the thermal, electrical and mechanical properties of PNCs were observed by Wang et al. (Wang 2013). Thus, characterization of nanotube length is a key step in both experimental and numerical modelling. Experimental studies have been conducted to investigate the length distribution of CNTs, including SWNTs (Wang 2006) and MWNTs (Cheng 2011). Some progress has been made with in situ techniques, which typically only give an average length and little information about the distribution (Zhou 2004, Kukovecz 2005). On the other hand, direct imaging techniques are more time consuming but typically

give more information. In particular, atomic force microscope (AFM) appears to be the most useful technique among different imaging approaches.

In the experimental work by Wang et al. (Wang 2006), they developed a simple and efficient means of quantifying a large population of CNT lengths (i.e., sample size n = 651) using AFM and SIMAGIS software. The length analysis module SIMAGIS provided automatic analysis AFM images of CNT and precise measurements of CNT length. In their work, the lengths were extracted and plotted in a histogram. It was obtained that the overall shape of the histogram could be characterized with either Weibull or log-normal distribution. The probability plots were generated for these two competing distributions to identify the one provided the better fit of the measured CNT length. Wang et al. provided the probability plots of Weibull and log-normal distribution for comparison. The Weibull probability plot generated a much straighter line than the log-normal plot with a negligible amount of points deviating very little from the straight line. In other words, only a few measurements departed from the specified distribution (i.e., Weibull distribution). Thus, the Weibull distribution, as in Equation 2.4, was used in order to realistically describe the length distribution of CNTs.

$$f(x) = abx^{b-1}e^{-ax^b} \qquad (2.4)$$

where a is the scale parameter and b is the shape parameter. Both of these parameters can be estimated by maximum likelihood estimation.

2.1.6 Effects of CNT alignment on PNCs' electrical properties.

Recent experimental studies have shown that the alignment of CNTs was a crucial morphology parameter affecting the electrical properties of PNCs. In general, the alignment of CNTs in polymer matrices can be controlled at different stages of the fabrication process. Firstly, an isotropic alignment of CNTs can be achieved by growing homogeneous CNT arrays on substrates using chemical vapor deposition before the fabrication of PNCs. On the other hand, it was reported that the CNTs dispersed in polymer matrices were aligned by applying magnetic/electrical fields (Oliva-Aviles 2011) or mechanical stretching and compression of polymers (Akima 2006) during fabrication of PNCs. In addition to these techniques, other approaches achieved tailored alignment of CNTs in polymers by adjusting draw ratio in stretching process (Zamora-Ledezma) or field strength and curing time (Moaseri 2014).

In the work by Du et al., the degree of CNT alignment satisfy the Lorentz distribution, which is characterized by the full width at half maximum, namely FWHM, (Du 2005). More specifically, they characterized the degree of CNT alignment using small-angle x-ray scattering fiber diagram. The parameter, FWHM, was introduced in their work to describe the CNT alignment quantitatively. Increasing FWHM from 0^0 (perfectly aligned) to 180^0 (isotropic) corresponded to decreasing the degree of CNT alignment. Interestingly, at fixed 2 wt.% CNT loading, the electrical conductivity of PNCs showed a sharp increment with respect to the degree of CNT alignment. It was observed that the electrical conductivity increased dramatically, from 6.5×10^{-11} to 4.4×10^{-6} S/cm, as the FWHM varied from 20^0 to 36^0. The hypothetical explanation was provided by Du et al.. When the CNTs were highly aligned, they rarely touch each other and thus did not form conductive path at small loading

(<3 wt.%). Consequently, the electrical conductivity was relatively low, comparing to the cases with lower degree of CNT alignment, when CNTs were highly aligned at small loading. Upon decreasing the degree of alignment (i.e., increasing FWHM), the CNTs started to contact each other, until the FWHM approached a critical value where the CNTs formed the conductive paths. Such percolation phenomenon of increasing FWHM was similar to the aforementioned percolation phenomenon when increasing the CNT loading. From the study conducted by Du et al., the electrical conductivity showed a non-monotonic dependence on the extent of CNT alignment and reached a maximum at a specific orientation (Du 2005).

Besides experimental work, numerical works were also conducted using two-dimensional (Du 2005), pseudo three-dimensional (Behnam 2007), and three-dimensional models (White 2009, Bao 2011), in attempt to determine the effect of CNT alignment on the electrical conductivity of PNCs. In particular, Bao et al. used a 3D random resistor network model with consideration of both intrinsic and contact resistances. The CNT alignment was controlled by setting the maximum alignment angle θ_{max}. As shown in Equations 2.5, the azimuthal angle φ_i and polar angle θ_i were generated randomly within their own range [0, 2π] and [$-\theta_{max}$, θ_{max}], respectively.

$$\varphi_i = 2\pi \cdot rand \tag{2.5a}$$

$$\cos\theta_i = (1-\cos\theta_{max}) \times rand + \cos\theta_{max} \tag{2.5b}$$

The effects of CNT alignment were investigated in the work conducted by Bao et al. qualitatively (Bao 2011). Firstly, parallel or almost parallel CNTs were less likely to contact each other and thereby difficult to form the connective paths (i.e., less conductive paths),

which was consistence with the aforementioned experimental study by Du et al.. On the other hand, reducing the degree of CNT alignment would lead to increment in the length of the conductive paths (i.e., longer conductive paths). Consequently, these two mechanisms had counter effects on electrical conductivity of PNCs. Maximum electrical conductivity was obtained in an optimal degree of CNT alignment.

2.2 Piezoresistivity of PNCs

PNCs with improved electrical conductivity are considered as emerging materials for highly sensitive strain sensor, due to the strain-induced resistivity change behaviour, namely piezoresistivity (Alamusi 2011). Recently, there have been experimental and numerical studies on the piezoresistivity of PNCs. In this section, the piezoresistive behaviour of PNCs will be first discussed, followed by the recent modeling schemes for PNCs' piezoresistivity. Then, the modeling on the fiber reorientation model is reviewed.

2.2.1 Piezoresistive behaviour of electrically conductive PNCs

The electrically conductive PNCs were increasingly being considered as promising alternatives to conventional smart materials. Recent experimental studies have been conducted to investigate the strain-induced changes in the resistance of PNC (i.e., Piezoresistivity).

Park et al. investigated the change in electrical resistances of polyethylene oxide (PEO)/multi-walled carbon nanotubes (MWNTs) nanocomposites subjected to different levels of strain at different MWNTs loadings (i.e., 0.56 vol.% and 1.44 vol.%). Linear relationship between the PNC's resistance and applied strain was reported (Park 2008). The

unique and repeatable strain-induced electrical resistance changes were observed at different loading of MWNTs. The overall pattern of electrical resistance change versus applied strain for the specimens of different volume fraction of MWNTs consisted of a linear region followed by nonlinear behaviour. In the linear region, it was hypothesized that the contact of MWNTs inside polymer matrix was maintained during stretching of the film (i.e., applying the external strain). However, after passing the critical strain, the contact of MWNTs was hypothesized to be broken down in non-linear region; and electron tunneling played a dominant role within this region. Park et al. concluded that such linear relationship between applied strain and the electrical resistance changes of PEO/MWNT specimens permitted these materials to be used as strain sensors in many applications.

Similarly, Fernberg et al. revealed that the electrical resistance of CNTs doped epoxy depended linearly on the applied strain (Fernberg 2009). In their work, the electrical resistivity of PNC with 0.5wt.% MWNT loading linearly increased with increasing strain, until ultimate failure of the specimen which occurred at the loading above 1.6% strain. Furthermore, they identified three different mechanisms contributing to the strain-induced resistance changes of the specimen, which are (a) geometrical changes of the specimen, (b) piezoresistive material response, and (c) microstructural damage.

Extensive experimental studies, including but not limited to the aforementioned studies, have been conducted to study PNCs' piezoresistivity and they provided invaluable insights in the piezoresistive behaviours of PNCs. In general, the measured piezoresistivity of PNCs were qualitatively attributed to three hypothetical mechanisms: (i) reconfiguration of CNTs conductive network in the PNC; (ii) change in tunneling resistance at CNTs junctions;

and (iii) change in the intrinsic electrical resistance of CNTs (Alamusi 2011). However, fundamental understanding of the governing mechanisms contributed to the piezoresistive behaviours in PNCs filled with CNTs has yet been elucidated.

2.2.2 Modeling piezoresistivity of PNCs.

Comparing with the experimental studies mentioned in the previous section, to author's best knowledge, there have been very limited theoretical or numerical studies on the piezoresistive behaviour of PNCs filled with CNTs. Up to date, only a few numerical modeling studies were focusing on the investigation of the working mechanisms of PNCs' piezoresistivity. Pham et al. applied an empirical model, based on the percolation theory, to investigate the effects of conductive network density and tunneling distance on sensitivity of PNCs' piezoresistivity (Pham 2008). They discovered that piezoresistivity increased significantly by having the filler content approach the percolation threshold. Oliva-Avilés et al. proposed an analytical model to evaluate the effects of CNT deformation and its influence on PNCs' piezoresistivity (Oliva-Avilés 2011). It was discovered that the strain-induced reconfiguration of CNT conductive network was the main governing factor to PNC's piezoresistivity, while the deformations of CNTs in length or diameter were negligible.

Besides the empirical model, 2D and 3D modeling in PNCs' piezoresistivity were performed by several researchers. In the work by Theodosiou et al., the 2D and 3D percolation models were used to numerically study the piezoresistive behaviours of PNCs (Theodosiou 2010). In the model, the percolation probability was determined as number of percolating CNTs that contributed to the conductive network over the total number of CNTs. In their work, the effect of applied strain on such percolation probability was revealed. They

reported that the piezoresistive behaviours were dominated by piezoresistive response of CNTs themselves within the strain range of 3.0%, while the effect of deformation of the percolation conductive network was negligible. However, in their work, the simulated results of PNCs' percolation threshold varied from experimental results. Furthermore, the validation of simulated PNCs' piezoresistivity was absent.

Hu et al. conducted numerical simulation to understand the piezoresistivity of PNCs. The developed model considered the tunneling effects when building the conductive network. The tunneling distance and thereby the tunneling resistances between CNTs were updated based on the rigid body movement of the CNTs under applied strain. They reported that the tunneling effect played a dominating role in piezoresistivity, while the contribution of the network breakup was not significant under small strains (i.e., 1.0%). Moreover, the tunneling resistance increased exponentially with the tunneling distance which was hypothetically increased under external strain. Consequently, they concluded that the strain-induced resistance change was dominated by the tunneling effect between contacting CNTs, instead of the breakup of the conductive network. However, nonlinear piezoresistivity was obtained in their simulation which was different to most of experimental works. Meanwhile, the direct evidences, such as the degree of the increment in tunneling resistance and the degree of breakup of the conductive path, lacked when they went to the aforementioned conclusion.

While different analytical and numerical studies have attempted to explain the piezoresistivity of PNCs from different perspectives, there is no systematical quantitative analysis that decouples the effects of different governing factors on PNC’s piezoresistivity,

including (i) destruction of CNT conductive networks; (ii) reorientation of CNTs; (iii) alternation of CNT conductive networks; (iv) variation in tunneling resistance; and (v) change in intrinsic resistance along CNT in the conductive paths.

2.2.3 Fiber reorientation model

Fiber reorientation model can be applied to the composite system with the aim of predicting the relation between the applied strain and the reorientation of conductive short fibers (i.e., CNTs). Such model realistically represented the strain-induced reconfiguration of CNTs conductive network within the polymer matrix (Taya 1998). Furthermore, such model can help to reveal the governing factors of PNCs' piezoresistive behaviours when the strain applied, such as reorientation of CNTs, destruction of CNT conductive network and alternation of CNT conductive network.

As discussed by Taya et al., the orientation and relocation of fibers in an elastomeric composite were expected to take place under applied strain (Taya 1998). Consequently, if the microstructure of conductive short fibers was initially percolating, the percolating microstructure was degenerated to less- or non-percolation network as the applied strain increases. In the fiber reorientation model presented by Taya et al., it was assumed that upon incremental uniaxial straining along the *x* axis, the changes in the orientation and location of a short fiber (i.e., CNT) were determined based on the affine transformation, which assumed that the length components of a fiber in particular direction (i.e., length components in *x*, *y* and *z* axes) would change by the same ratio as the corresponding dimensions (i.e., *x*, *y* and *z* directions) in the matrix. In the 3D modeling for the piezoresistivity of PNCs, the fiber

reorientation model would be used to realistically represent the strain-induced morphological changes in CNT conductive network.

2.3 Summary

In summary, this chapter presents the extensive experimental and numerical studies on the electrical conductivity of nanocomposites made from insulating polymers filled by CNTs have been conducted by researchers. The concept of percolation phenomenon in CNT-polymer PNC has been discussed. While researchers have progressively improved the models used to determine PNC's electrical conductivity, a number of shortcomings in existing modeling schemes were also discussed. As a result, it is important for researchers to develop new modeling schemes to determine PNC's electrical conductivity. One of the most important aspects is to improve the computational efficiency without compromising the accuracy of the simulation results.

Moreover, this chapter also provides a summary of the experimental and numerical studies of the piezoresistive PNC. Although different analytical and modeling studies have attempted to explore the piezoresistivity of PNCs from different perspectives, quantitative analyses on the effects of different microscopic governing factors on PNC's macroscopic piezoresistive behaviours were scarce. This led to a barrier to elucidate the structure-to-property relationship of piezoresistive PNC filled with CNT.

CHAPTER 3 Electrical Conductivity of PNCs

3.1 Theoretical framework

In the 3D simulation model, electrically conductive PNCs can be represented by a cuboid RVE of $L_x \times L_y \times L_z$ embedded with a random distribution of CNTs. A schematic of the cuboid RVE is shown in Figure 3.1. Electric current is considered to propagate from the left boundary surface (i.e., high voltage electrode) to the right boundary surface (i.e., low voltage electrode).

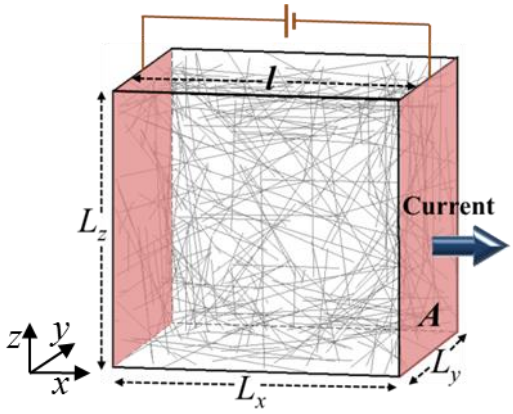

Figure 3.1 A schematic of CNTs randomly dispersed in a representative volume element

3.1.1 Cuboid representative volume element (RVE) of electrically conductive PNCs

Each CNT is considered as a "soft-core" capped cylinder as shown in Figure 2.3. Its axle is represented by a line segment starting from $(x_{i,1}, y_{i,1}, z_{i,1})$ and ending at $(x_{i,2}, y_{i,2}, z_{i,2})$. In order to model the random distribution of CNTs, the coordinates of the starting and ending points are generated by Equations (3.1) and (3.2), respectively.

$$x_{i,1} = L_x \cdot rand \tag{3.1a}$$

$$y_{i,1} = L_y \cdot rand \tag{3.1b}$$

$$z_{i,1} = L_z \cdot rand \tag{3.1c}$$

where *rand* is a uniformly distributed random number in [0,1].

$$x_{i,2} = x_{i,1} + L_{CNT} \cos\varphi_i \sin\theta_i \tag{3.2a}$$

$$y_{i,2} = y_{i,1} + L_{CNT} \sin\varphi_i \sin\theta_i \tag{3.2b}$$

$$z_{i,2} = z_{i,1} + L_{CNT} \cos\theta_i \tag{3.2c}$$

where L_{CNT} is the average length of the CNT; φ_i is the azimuthal angle; and θ_i is the polar angle.

The orientation of CNT_i is defined by the azimuthal and polar angles, which can be generated by Equations (3.3a) and (3.3b), respectively.

$$\varphi_i = 2\pi \cdot rand \tag{3.3a}$$

$$\cos\theta_i = (1 - \cos\theta_{max}) \times rand + \cos\theta_{max} \tag{3.3b}$$

where θ_{max} is the upper limit of the alignment angle (i.e., the angle between the CNT and the *x*-axis). θ_{max} equals to $\pi/2$ represents the case of PNCs with isotropically distributed CNTs without any preferential orientation; θ_{max} equals to zero represents the case of PNCs with all CNTs perfectly aligned in the direction of the current flow (i.e., the *x*-axis).

3.1.2 Electrical conductivity of PNCs represented by an individual cuboid RVE

In the simulation model, all the interconnecting CNTs that bridge the two electrodes in a RVE are identified to construct the random resistor network. Similar to the previous numerical studies (Hu 2008b, Bao 2011), two types of resistances in the percolating CNTs network are considered, namely the intrinsic resistance ($R_{intrinsic}$) along an individual CNT and the contact resistance ($R_{contact}$) between two CNTs. Referring to Figure 3.2, two CNTs are considered to be connected and form a continuous electrically conductive path when the shortest distance between them is shorter than the cut-off distance (d_{cutoff}). The intrinsic resistance along CNT_i, between $Node_k$ and $Node_l$, can be calculated by Equation (3.4).

$$R_{intrinsic,kl} = \frac{4l_{kl}}{\pi\sigma_{CNT}D^2} \tag{3.4}$$

where σ_{CNT} is the intrinsic electrical conductivity of the CNT; D is the diameter of the CNT; and l_{kl} is the distance between $Node_k$ and $Node_l$.

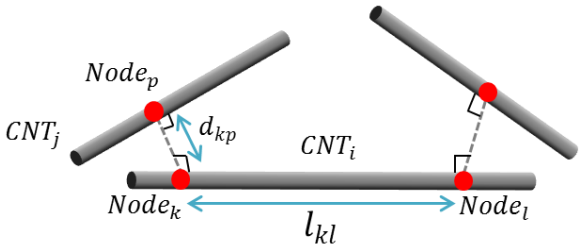

Figure 3.2 A schematic of CNTs' interconnection.

The contact resistance between CNT_i and CNT_j is induced by electron ballistic tunneling through the contact junction. The Landauer-Büttiker formula can be used to estimate the contact resistance (Buldum 2001), which depends on the shortest distance

between them (i.e., d_{kp}), which is shorter than d_{cutoff}. Its value can be determined by Equations (3.5a) through (3.5c).

$$R_{contact,kp} = \frac{h}{2e^2}\frac{1}{M\mathrm{T}} \tag{3.5a}$$

$$\mathrm{T} = \begin{cases} \exp\left(-\dfrac{d_{vdw}}{d_{tunnel}}\right) & \text{for } 0 \le d_{kp} \le D + d_{vdw} \\ \exp\left(-\dfrac{d_{kp} - D}{d_{tunnel}}\right) & \text{for } D + d_{vdw} \le d_{kp} \le D + d_{cutoff} \end{cases} \tag{3.5b}$$

$$d_{tunnel} = \frac{h}{2\pi}\frac{1}{\sqrt{2m_e\Delta\mathrm{E}}} \tag{3.5c}$$

where h is Planck's constant; T is the transmission probability for the electron to tunneling between CNTs through polymer; M is the number of conduction channels, which is dimensionless and related to CNT's diameter (Naeemi 2009); e is the charge of an electron; d_{vdw} is the van der Waals separation distance caused by the Pauli exclusion principle (Hertel 1998, Girifalco 2000), which limits the minimum distance between two CNTs; d_{tunnel} is the tunneling characteristic length; m_e is the mass of an electron; and ΔE is the height of energy barrier (Simmons 1963).

After identifying the random resistor network of CNTs in the RVE as well as calculating the $R_{intrinsic}$ and $R_{contact}$ of all CNTs in the network, a conductance matrix is constructed to represent the network using the Kirchhoff's circuit laws (Knudsen 2006). The equivalent conductance of this conductive network (i.e., denoted as G_{RVE}) can be obtained

using the Gaussian decomposition method. Consequently, the PNC's electrical conductivity, σ, can be obtained by Equation (3.6).

$$\sigma = G_{RVE}\frac{l}{A} = G_{RVE}\frac{L_x}{L_y L_z} \tag{3.6}$$

where l is the distance between the left and right boundary surfaces; and A is the cross-sectional area of the RVE.

3.1.3 Electrical conductivity of PNCs by considering the interconnectivity of CNTs across the RVEs' boundary surfaces

Figure 3.3 shows a schematic that illustrates the interconnectivity of CNTs across a boundary surface between adjacent RVEs. It is apparent that the simulation procedures described in the previous sections will neglect the highlighted conductive pathways generated by CNTs across the boundary surface (i.e., path AA' and BB' in Figure 3.3). This would lead to an underestimation of the PNC's and an overestimation of the PNC's ϕ_c by the model, especially for a relatively small RVE. One possible solution to circumvent this problem is to use a RVE that is sufficiently large such that the error caused by the ignorance of the cross-boundary CNTs would reduce. However, such approach will significantly increase the computation cost (i.e., time and memory) to run the simulation. Therefore, a new model is developed in this work to account for the electrical conductivity contributed by the interconnecting CNTs in adjacent RVEs across the boundary surfaces. Without adopting the "cut-and-relocate" approach to handle CNTs penetrating the RVE's boundary, it is possible to avoid the unnecessary bias that immediately increases the number of CNTs penetrating

the two terminals. This will help filling a loophole existed in previous simulation models, leading to more realistic representation of electrically conductive PNC filled embedded with three-dimensional CNT networks. In other words, the new model will enhance the research on the structure-to-property relationships of these PNC, and thereby facilitate the development of smart and multifunctional PNC with tailored electrical properties.

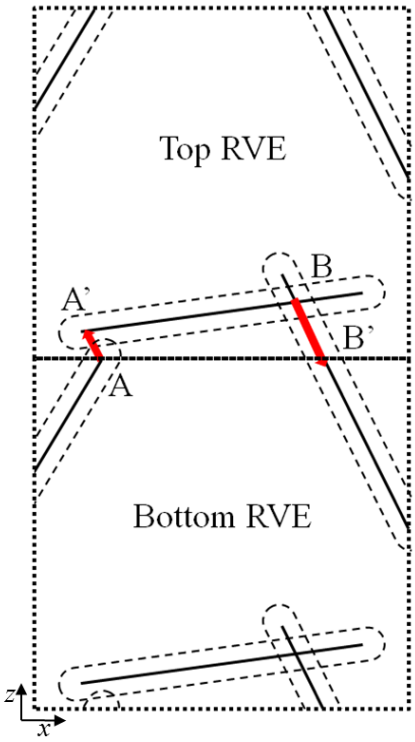

Figure 3.3 A schematic of interconnectivity of CNTs across the boundary surface of adjacent RVEs.

In the new model, the CNTs are distributed in an $L_x \times L_y \times 2L_z$ rectangular cuboid, consisting of a RVE on top of another, as illustrated in Figure 3.4. The electrical conductance of the rectangular cuboid, the top RVE, and the bottom RVE (i.e., G_{rect}, $G_{RVE,top}$, and $G_{RVE,bottom}$) can be calculated independently by the procedures discussed in the previous sections. In

Figure 3.4, the CNTs penetrating across the boundary surface are highlighted. Among them, some CNTs contributing to the electrically conductive pathways in the rectangular cuboid cell may contribute neither to the electrically conductive pathways in the top RVE nor to the bottom RVE. In other words, they are independent of the CNT networks contributed to $G_{RVE,top}$ and $G_{RVE,bottom}$. These extra electrically conductive pathways would lead to additional electrical conductance in both the bottom boundary surface of the top RVE and the top boundary surface of the bottom RVE.

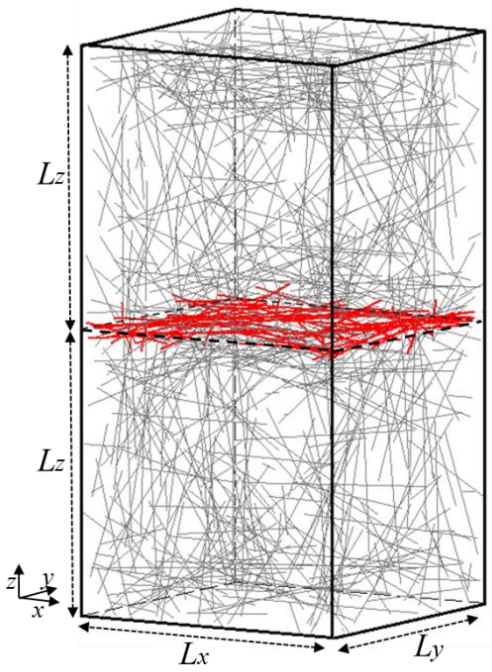

Figure 3.4 CNTs distributed in a rectangular cuboid (note: CNTs penetrating across the boundary surface are highlighted).

Considering the isotropic random distribution of CNTs, the additional electrical conductance in both the bottom boundary surface of the top RVE and the top boundary surface of the bottom RVE can be approximated to equal each other, and they can be denoted

as $G_{boundary}$. These additional and independent pathways ($G_{boundary}$), bridging the left boundary surface (i.e., high voltage electrode) and the right boundary surface (i.e., low voltage electrode), are parallel to the CNT networks in the cores of the top RVE ($G_{RVE,top}$) and the bottom RVE ($G_{RVE,bottom}$). Hence, the relationship among G_{rect}, G_{RVE}, and $G_{boundary}$ (i.e., the average of $G_{RVE,top}$, and $G_{RVE,bottom}$) can be expressed by Equation (3.7).

$$G_{rect} = 2G_{RVE} + 2G_{boundary} \tag{3.7}$$

Similarly, the front and back boundary surfaces of each cuboid RVE would also contribute to additional electrical conductance of the RVE. All together, the conductance of an individual cuboid RVE, accounting for the additional electrical conductance contributed by the four boundary surfaces parallel to the direction of electric current, can be determined by Equation (3.8).

$$G_{adj} = G_{RVE} + 4G_{boundary} \tag{3.8}$$

where G_{adj} and G_{RVE} are the equivalent electrical conductance with and without considering the additional conductance contributed by the interconnecting CNTs across the boundary surfaces, respectively.

Combining Equations (3.7) and (3.8), the equivalent electrical conductance of an individual RVE can be expressed as Equation (3.9).

$$G_{adj} = 2G_{rect} - 3G_{RVE} \tag{3.9}$$

Replacing G_{RVE} by G_{adj} in Equation (7), PNC's electrical conductivity (σ_{adj}) after accounting for the contribution of the interconnecting CNTs across the boundary surfaces of adjacent RVEs to the equivalent electrical conductance, can be calculated using Equation (3.10).

$$\sigma_{adj} = \left(2G_{rect} - 3G_{RVE}\right)\frac{L_x}{L_y L_z} \tag{3.10}$$

3.2 Results and discussion

Using the newly developed model, Monte Carlo simulations were conducted to investigate the effects of RVE's dimensions, PNC's thickness, and CNT's alignment on PNCs' ϕ_c and σ. Simulation results were compared with experimental data and other simulation works to verify the validity of the models. Studies were also conducted to confirm the enhancement in computational efficiency by the refined modelling scheme using smaller RVEs without compromising the accuracy of the simulation results. Table 3.1 summarizes the values of some key physical parameters used in this work. The value of d_{vdw} was based on the Van de Waals interaction between carbon nanotubes (Hertel 1998, Girifalco 2000). The value of d_{cutoff} was based on the threshold distance between CNTs, over which the transmission probability would be less than 10^{-6} (Alamusi 2011). ΔE depends on the polymer matrix (Hu 2008b). Its value was chosen according to previous numerical studies on the electrical conductivity of PNCs (Bao 2011, Hu 2008b). This also ensures a fair comparison

between our simulation results in this thesis to those based on other models reported in literatures (Bao 2011, Hu 2008b) in the later sections.

Table 3.1 Physical Parameters used in simulation

Physical Parameters	Value	Unit
Van der Waals separation distance (d_{vdw}) [35, 36]	3.4	Å
Cut-off distance (d_{cutoff}) [23]	1.4	nm
Energy barrier (ΔE) [23, 39]	1.0	eV

3.2.1 Effects of RVE's dimensions on the simulation results of electrical conductivity

Various studies have demonstrated that the simulation results of PNC's σ using the 3D resistor network model are sensitive to the dimensions of the RVE. In order to suppress the effect of RVE's size on the simulation results, Hu *et al.* (Hu 2008a, Hu 2008b) showed that a cuboid RVE of 25 μm × 25 μm × 25 μm was needed to simulate ϕ_c and σ of PNCs filled with CNTs with an average length of 5 μm in order to achieve numerical convergence. However, the relatively large RVE also led to a surge in computational burden. In order to demonstrate the sensitivity of the simulation results based on the refined model on the RVE's dimensions, a series of simulations using RVEs with different sizes were conducted and the results are shown in Figures 3.5(a) through 3.5(d). As a case example, the physical parameters of CNTs used in the simulations were the same as those used by Hu *et al.*. Hence, the length and diameter of CNTs were set to be 5 μm and 50 nm, respectively. In addition, the number of

conduction channels (M) and intrinsic electrical conductivity of a CNT (σ_{CNT}), were chosen to be 460 and 1×10^4 S/m, respectively (Naeemi 2009).

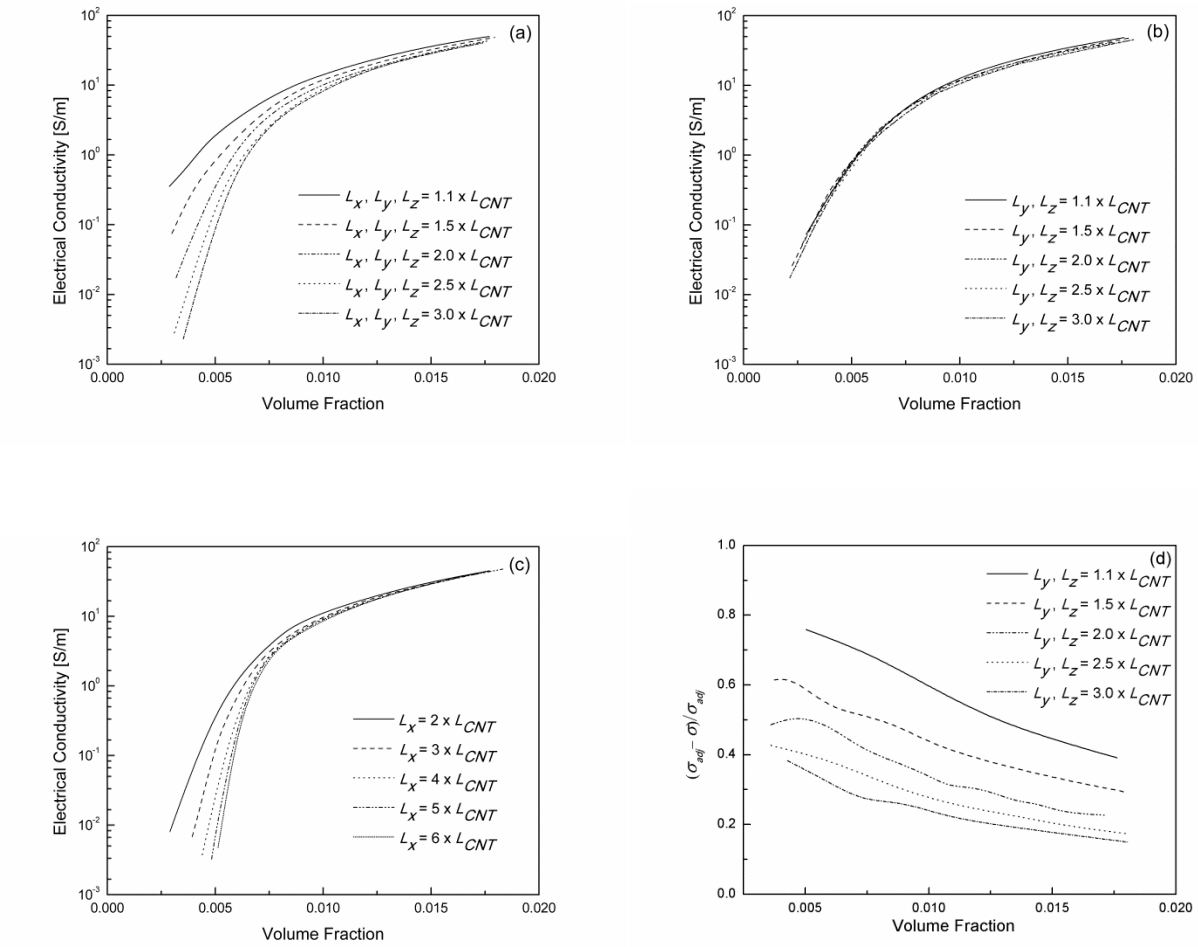

Figure 3.5 Simulation results of PNC's σ_{adj} at different CNT loadings based on (a) cubic RVEs with different dimensions; (b) cuboid RVEs with fixed L_x (i.e., $1.5 \times L_{CNT}$) but varying L_y and L_z; (c) cuboid RVEs with fixed L_y and L_z (i.e., $1.5 \times L_{CNT}$) but varying L_x; and (d) relative difference of simulated σ_{adj} and σ with varying L_y and L_z.

Figure 3.5(a) depicts that the simulation results of PNCs' σ_{adj} were sensitive to the changes in cubic RVEs' dimensions at low CNT loadings (i.e., $\phi < 0.01$). It is apparent that

simulated σ_{adj} at different CNT loadings converged as the RVEs' dimensions increased. Regardless of the RVEs' sizes, the PNCs' σ_{adj} rapidly increased at low CNT loadings and approached to a plateau as ϕ increased. The general trends were consistent with the numerical works conducted by Hu *et al.* (Hu 2008b). Figures 3.5(b) and (c) plot the effect of simultaneously varying L_y and L_z while fixing L_x, and that of varying L_x while fixing L_y and L_z, respectively, on PNCs' σ_{adj}. These results would help to decouple the influence of varying the dimension parallel to the direction of current flow from that of varying the dimensions perpendicular to the current flow. As shown in Figure 3.5(b), when L_x was fixed to $1.5 \times L_{CNT}$, PNCs' σ_{adj} were unaffected by varying L_y and L_z, regardless of the CNT loadings. In contrast, Figure 3.5(c) reveals that when L_y and L_z were fixed, the simulated PNCs' σ_{adj} were sensitive to the change of L_x at low CNT loadings (i.e., $\phi < 0.01$), while they were virtually indifferent at higher CNT loadings. The figure suggested that the simulation results started to converge when L_x was greater than or equal to $4.0 \times L_{CNT}$. Figure 3.5(d) shows the relative difference between the simulation results with and without considering the contribution of interconnecting CNTs across the boundary surfaces (i.e., σ_{adj} and σ) when different L_y and L_z were used. The relative difference reduced as L_y and L_z increased. In other word, the contribution made by the interconnecting CNTs across the boundary surfaces to PNC's electrical conductivity was more significant at smaller L_y and L_z.

Since varying L_y and L_z while fixing L_x were proven to have negligible influence on the simulation of PNCs' σ, it is possible to significantly improve the computational efficiency of the Monte Carlo simulation by reducing L_y and L_z. Figure 3.6 compares the simulation time per run for the case using RVE with all dimensions equaled to $4.0 \times L_{CNT}$ with that for the case

using RVE of L_x equaled to 4.0 × L_{CNT} and L_y and L_z equal to 1.1 × L_{CNT}. While the simulation results were virtually similar in both cases, the computation time was found to be significantly shortened by reducing L_y and L_z from 4.0 × L_{CNT} to 1.1 × L_{CNT}, especially at higher CNT loadings. Therefore, the refined modelling scheme, which uses a relatively small cuboid RVE, would substantially improve the simulation efficiency without compromising the desired numerical accuracy.

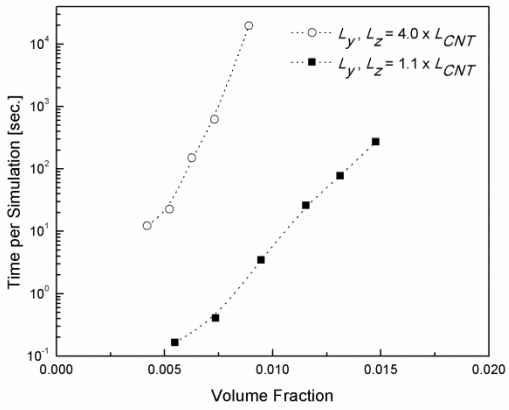

Figure 3.6 Comparison of simulation times per run using different lengths of L_y and L_z (note: L_x is fixed at 4 × L_{CNT}).

3.2.2 Model validation and comparison with experimental works and other models

In order to verify the validity of the new model developed in this work, simulation results of σ_{adj} for PNCs filled with CNTs of different grades (i.e., different dimensions and physical properties) were compared to experimental results (Ono 2006, Hu 2008b, Krause

2011). Figure 3.7(a) plots the comparison of simulated PNCs' σ_{adj} with experimental measurements for PNCs filled with multi-walled carbon nanotubes (MWNTs) of L_{CNT} and D equaled to 5 μm and 50 nm, respectively. Unlike most of other numerical studies that selected values of CNT's σ_{CNT} within the typical range reported in literature, the simulation in this work considered the dependence of σ_{CNT} and M on the dimensions of CNTs (Naeemi 2009) in order to conduct more realistic simulation. These two parameters were determined to be 2.1×10^3 S/m and 460, respectively. It can be observed that the numerical predictions of PNCs' σ_{adj} at different CNT loadings showed good agreement with experimental results. Figure 3.7(b) illustrates the comparison of simulated PNCs' σ_{adj} with experimental data for PNCs filled with MWNTs of smaller dimensions yet higher aspect ratio. Distribution of L_{CNT} was characterized by Krause *et al*. using a normalized frequency versus CNT's length bar chart (Knudsen 2006). In our simulation work, the Weibull Distribution (Wang 2006), as Equation (3.11), was used to represent such distribution of L_{CNT}.

$$f(x;\lambda,k) = \begin{cases} \frac{k}{\lambda}\left(\frac{x}{\lambda}\right)^{k-1} e^{-\left(\frac{x}{\lambda}\right)^k} & x \geq 0, \\ 0? & x < 0, \end{cases} \tag{3.11}$$

where λ is the scale parameter and k is the shape parameter.

The average length and diameter of the MWNTs were determined to be 1.603 μm and 9.5 nm, respectively. The resultant σ_{CNT} and M were equal to 900×10^3 S/m and 87, respectively (Naeemi). Similar to the previous case, the PNCs' σ_{adj}, numerically predicted by the new model and simulation scheme, showed good agreement with the experimental measurements. In short, the good agreement between the simulation results and the

experimental results for the electrical conductivity of PNCs filled with different grades of MWNTs suggest that the refined model and simulation scheme can be used as a strategic tool to design CNT loadings and CNTs' degree of alignment to tailor the PNCs' ϕ_c and σ. This will facilitate the identification of structure-to-property relationship of electrically conductive PNC embedded with three-dimensional CNT network. Moreover, it will enhance the research and development of smart and multifunctional PNC with tailored electrical properties.

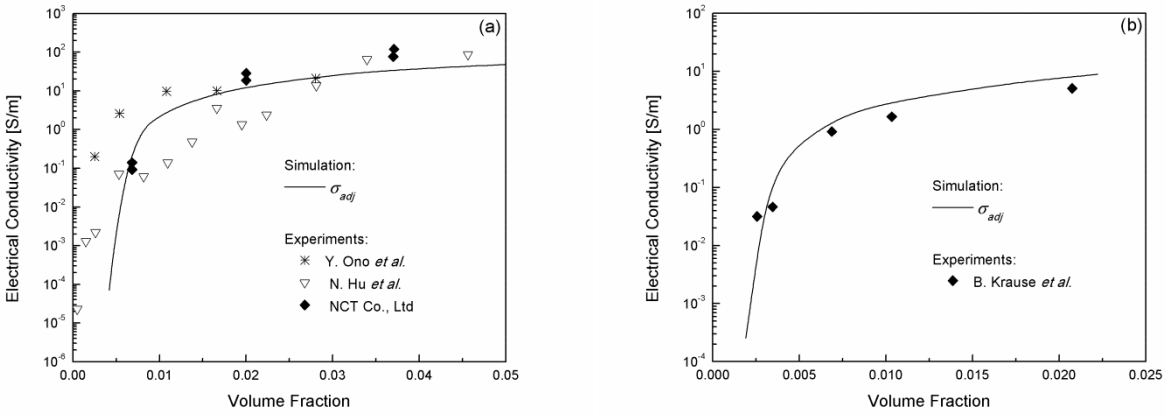

Figure 3.7 Comparison of simulation results of PNCs' σ_{adj} with existing experimental data obtained by: (a) Y. Ono et al., N. Hu et al., and NCT Co. Ltd.; and (b) B. Krause et al..

Simulations results obtained using the refined model were also compared with other numerical studies, based on the 3D random resistor network model, conducted by Hu *et al.* (Hu 2008b) and Bao *et al.* (Bao 2011). The comparisons are plotted in Figures 3.8(a) and 3.8(b). Since Hu *et al.* employed a cubic RVE with side length of 5 × L_{CNT}, the RVE used herein had L_x equaled to 5 × L_{CNT}, while L_y and L_z equaled to 1.1 × L_{CNT} in order to ensure a fair comparison. The reduced lengths in both L_y and L_z were justified by the insensitivity of the simulation results to the changes in these two dimensions. Bao *et al.*, on the other hand,

employed a cubic RVE of its side length equal to 1.1 × L_{CNT}. Therefore, to ensure a fair comparison, the simulation results to be compared with their results were generated based on two cases: (i) a RVE of identical dimensions $L_x = L_y = L_z = 1.1 \times L_{CNT}$; and (ii) a RVE of L_x equaled to 4 × L_{CNT}, while L_y and L_z equaled to 1.1 × L_{CNT}.

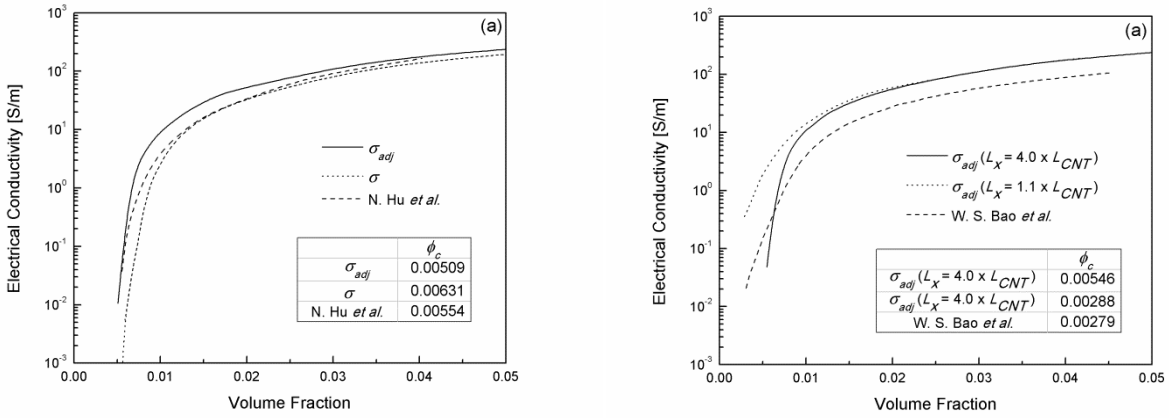

Figure 3.8 Comparison of simulation results with other numerical studies: (a) N. Hu et al., (b) W. S. Bao et al., based on the 3D resistor network model.

Figure 3.8(a) illustrates the comparison between the simulation results of σ and σ_{adj} and the predicted σ obtained by Hu *et al.* (Hu 2008b). The plot reveals that σ_{adj} (i.e., predicted electrical conductivity by considering interconnecting CNTs at the boundary) was higher than σ (i.e., predicted electrical conductivity without considering interconnecting CNTs at the boundary) for PNCs with different CNT loadings; however, the difference between them reduced with increasing loads of CNT. This trend can be attributed to the establishment of sufficient number of electrically conductive paths in the PNC's core at higher CNT contents. In other words, the relative contribution of interconnecting CNTs across the RVE's boundary surface to the overall conductive network gradually decreased. Moreover, Figure 3.8(a) also reveals that the simulation results reported by Hu *et al.* were consistent with σ_{adj} and σ

simulated in this work at a wide range of CNT loadings. The similar values of ϕ_c are obtained. Nevertheless, obvious differences can be observed for PNCs with CNT's volume fraction either below ~0.013 or above ~0.03. At lower CNT loading (i.e., $\phi < 0.013$), by cutting the extruding portion of CNTs outside the RVE and relocating them onto the opposite boundary surfaces, Hu *et al.* unintentionally generated bias on the random distribution of CNTs and resulted in a higher than usual number of CNTs in contact with the two electrodes (i.e., the left and right boundaries of RVE). This led to a higher simulated than our predicted σ. At higher CNT loading (i.e., $\phi > 0.03$), the error caused by the ignorance of the contact resistance among interconnecting CNTs by their work became more significant as the number of interconnecting CNTs in the random resistor network increased. Therefore, it would lead to an overestimation of PNCs' σ, which resulted in a simulation result higher than the predicted σ in this work. This was also consistent with the later work by Hu *et al.* (Hu 2008b) that demonstrated the significance of tunneling effect on PNCs' σ.

Figure 3.8(b) illustrates the comparison between the simulation results by Bao *et al.* (Bao 2011) and the simulated σ_{adj} based on RVEs of the aforementioned two dimensions. Comparing the trends among the three plots, it is worthwhile to note that the trends of our calculated σ_{adj} using a cubic RVE with its side length equaled to $1.1 \times L_{CNT}$ was similar to the simulated σ reported by Bao *et al.* This also resulted in very similar ϕ_c between their work (i.e., $\phi_c = 0.00279$) and this study (i.e., $\phi_c = 0.00288$). However, it is apparent that their predicted σ was consistently lower than the simulated σ_{adj} in this work at all CNT loadings. Using the "cut and relocate" approach, the CNT's length, and thereby the aspect ratio in their relatively small RVE would be decreased significantly. This would reduce the probability to

generate an electrically conductive pathway, leading to lower predicted values of PNC's σ. Moreover, obvious difference can be seen when comparing their predicted σ with the simulated σ_{adj} based on a RVE with L_x equaled to 4 × L_{CNT}. By increasing L_x to 4 × L_{CNT}, the ϕ_c of the PNC increased dramatically (i.e., ϕ_c = 0.00546) because of the lower probability to develop a continuous conductive channel along a longer path. This again confirmed that a sufficient length in the direction of current flow is needed to achieve numerical convergence.

3.2.3 Effect of the distance between two electrodes in a RVE on percolation threshold

As previously shown in Figure 3.5(c), the simulated PNC's σ_{adj} was predominantly influenced by the change in L_x (i.e., the distance between two electrodes in a RVE), especially at low CNT loadings (i.e., $\phi < 0.01$). Such influence was negligible at higher CNT loadings. To more clearly demonstrate the effect of changing L_x on the formation of conductive CNT network in a polymer matrix, the power law fitting based on the percolation theory (i.e., Equation (2.1)) was applied to determine the PNC's ϕ_c for varying L_x was applied to determine the PNC's ϕ_c for varying L_x, and the results are plotted in Figure 3.9. It is apparent that ϕ_c increased as the volume of the RVE increased by only increasing L_x. In contrast, when the volume of the RVE increased by simultaneously increasing both L_y and L_z, the PNC's ϕ_c remained relatively constant. Overall, it is reasonable to conclude that ϕ_c has a positive relationship with L_x, but is virtually independent of L_x and L_z. This finding on the effect of increasing L_x on ϕ_c is consistent with the experimental observations reported by Fu *et al.* (Fu 2009). It was proven experimentally that PNC's ϕ_c would be influenced by the test sample's

thickness, across which the PNC's σ was measured. Their experimental measurements revealed that PNC's σ increased significantly with the thickness of the PNC sample.

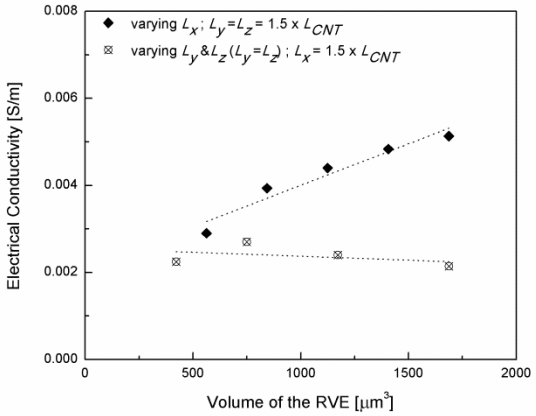

Figure 3.9 Calculated percolation threshold using different RVEs, cuboid RVEs with fixed L_y and L_z (i.e., 1.5 × L_{CNT}) but varying L_x; and cuboid RVEs with fixed L_x (i.e., 1.5 × L_{CNT}) but varying L_y and L_z.

The positive relationship between L_x and PNC's ϕ_c can be explained by considering the probability of having the minimum number of CNTs to construct an electrically conductive pathway across the two terminals. Under the percolation theory, ϕ_c is the critical concentration of CNTs at which the formation of the first conductive CNT pathway, bridging the two electrodes across the RVE (i.e., across $L_{x,}$). Increasing L_x means a longer separation distance between the two electrodes, leading to the needs of a larger number of CNTs to construct a conductive path. For a given loading of randomly dispersed CNTs in the RVE, the probability of sequentially interconnecting CNTs to form a continuous path to bridge the two electrodes decreases exponentially as the minimum required number of CNTs increases. For example, for a RVE with L_x equals to 10 μm, it requires at least two 5 μm-long CNTs to form

a conductive path bridging the two electrode surfaces. If L_x of the RVE is increased to 15 μm, a minimum of three 5 μm-long CNTs would be needed to achieve the same. The probability of three CNTs to interconnecting one another can be determined by considering the overall probability of two independent events to occur simultaneously. First, two CNTs need to be interconnected to create a conductive channel. Consequently, a third CNT will need to interconnect with the end of this two-CNT channel. It is apparent that the probability of forming a three-CNT conductive pathway (i.e., consists of two independent events) is lower than that of forming a two-CNT conductive pathway. Therefore, it would be less likely for a small number of CNTs to generate a conductive pathway across the RVE with longer L_x. In other words, a higher concentration of CNTs would be required to construct an electrically conductive pathway, and thereby increasing the PNC's ϕ_c. On the other hand, increasing L_y and L_z only lead to the increase in the RVE's volume without affecting the probability of developing the first conductive path in the direction of the electric current flow.

3.2.4 Effect of CNTs' alignment on PNCs' percolation thresholds and electrical conductivity

Figures 3.10(a) through 3.10(c) plot the effect of CNTs' alignment on the PNCs' ϕ_c and σ_{adj}. The simulations were conducted using a RVE as described in Section 3.1. The alignment of CNTs was varied by setting the upper limits for the angle between CNTs and the x-axis (i.e., θ_{max}) in Equation (3.3b). Figure 3.10(a) shows that the simulation results of PNCs' σ_{adj} versus the degree of CNT alignment. For θ_{max} ranging for 30° (i.e., highly aligned) to 90° (i.e., perfectly random orientation), the PNC's σ_{adj} increased rapidly at low CNT loading, and increased gradually thereafter to a plateau with increasing CNT loadings. However, the

dependence of PNC's σ_{adj} on θ_{max} varied with CNT loadings. This changing relationship of σ_{adj} versus θ_{max} is clearly revealed in Figure 3.10(b). In order to maximize PNC's σ_{adj}, a higher degree of CNT alignment was favorable at higher CNT loadings, whereas more randomly oriented CNTs were beneficial at lower CNT loadings. Furthermore, the effects of CNTs alignment on PNCs' ϕ_c are shown in Figure 3.10(c). The simulation results show that ϕ_c decreased as θ_{max} increased (i.e., CNTs were more randomly oriented). These findings were consistent with the experimental studies conducted by Du *et al.* (Du 2005).

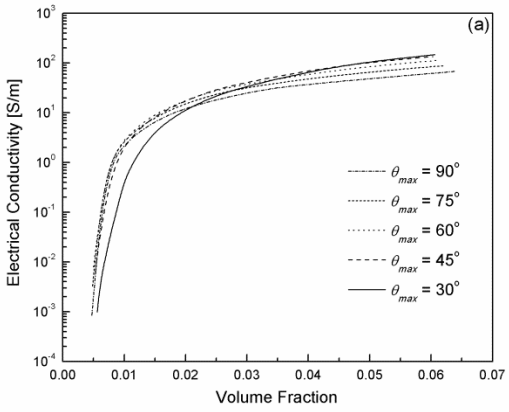

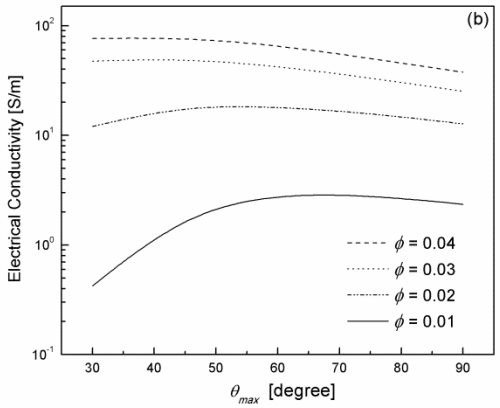

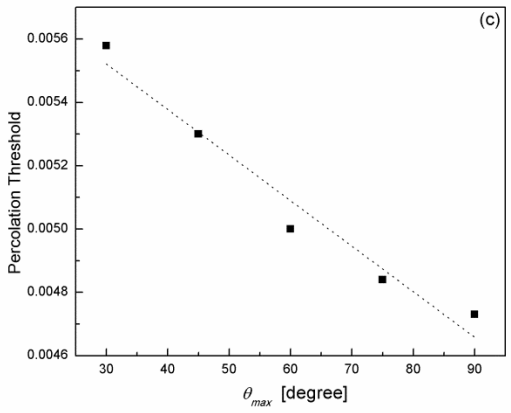

Figure 3.10 Calculated electrical properties of PNCs at different CNTs alignment, (a) electrical conductivity vs. volume fraction at different θ_{max}; (b) electrical conductivity vs. θ_{max} at different volume fraction; (c) percolation threshold vs. θ_{max}.

When CNTs are highly aligned, (e.g., θ_{max} = 30°), all CNTs are nearly parallel to each other. Thus, it is less probable for CNTs to interconnecting each other to form a conductive channel at small ϕ. In other words, a higher loading of CNTs would be required to form the first electrically conductive pathway, and thereby increasing PNCs' ϕ_c. On the other hand, for PNCs filled with high concentrations of CNTs, a large number of electrically conductive pathways would be formed easily in the polymer matrix. Along each of these numerous pathways, the conductance is governed by the length of the path (i.e., intrinsic resistance) and the number of CNT intersections (i.e., contact resistance) along the path. In PNCs filled with randomly-oriented CNTs, these conductive paths comprise of more CNTs, and thereby leading to longer pathways and more CNT-to-CNT intersections along these paths. As a result, the conductance of these paths would be lower, resulting in reduced PNC's σ_{adj} at higher CNT loadings. Combining the observations from Figures 3.10(a) through 3.10(c), it can be

concluded that highly aligned CNTs would help to maximize PNCs' σ with high CNT loadings; however, perfectly oriented CNTs would help to suppress PNCs' ϕ_c.

3.3 Concluding Remarks

A more realistic and efficient model to describe the three-dimensional carbon nanotube (CNT) networks in polymer nancomposites (PNCs) has been developed in this work. Compared to various existing random resistor models, the refined model accounts for the contribution of interconnecting CNTs across the boundary surfaces of the representative volume element (RVE). This avoid unnecessary biases in the spatial dispersion and length distribution of CNTs being caused by the "cut-and-relocate" approach adopted in typical models found in literatures. A series of Monte Carlo simulations, based on RVEs with different dimensions, have revealed that the simulated PNC's electrical conductivity is only influenced by the RVE's dimension parallel to the direction of the current flow. This leads to a more efficient simulation scheme of using RVEs with reduced length in dimensions perpendicular to the direction of the current flow. As a result, the computation cost of the Monte Carlo simulations can be suppressed significantly without compromising their accuracy. Using the improved model, electrical conductivity of PNCs filled with different grades of multi-walled carbon nanotubes were predicted, and the results demonstrated good agreement with those reported in existing experimental studies. It has also been shown that PNCs' percolation threshold (ϕ_c) increased with the distance between the two electrodes of the RVE. Through comparisons with other simulation models, the key differences and improvements of the refined model were elucidated. Furthermore, the effects of CNTs'

orientation on PNCs' ϕ_c and σ have been studied. Simulation results suggest that perfectly random orientation of CNTs lead to lower ϕ_c, while highly aligned CNTs along the direction of electric current lead to higher σ at high CNT loadings. In short, the new model being developed in this work would serve as a more realistic strategic tool to design optimal CNT loading and orientation to tailor the PNC's electric properties.

CHAPTER 4 Piezoresistivity of PNCs

4.1 Theoretical framework

The advanced 3D random resistor network model described in previous chapter has been extended to determine PNCs' piezoresistive behaviours through Monte Carlo simulations. A flowchart that overviews the simulation procedures is shown in Figure 4.1. The modeling of macroscopic piezoresistive behaviours, which are the relative changes in PNCs' electrical resistance under external strain (i.e., the ratio of deformation to the initial dimension of the material), can be decoupled to modeling of the electrical conductivity before/after applying strain and modeling the conductive network evolution under applying strain.

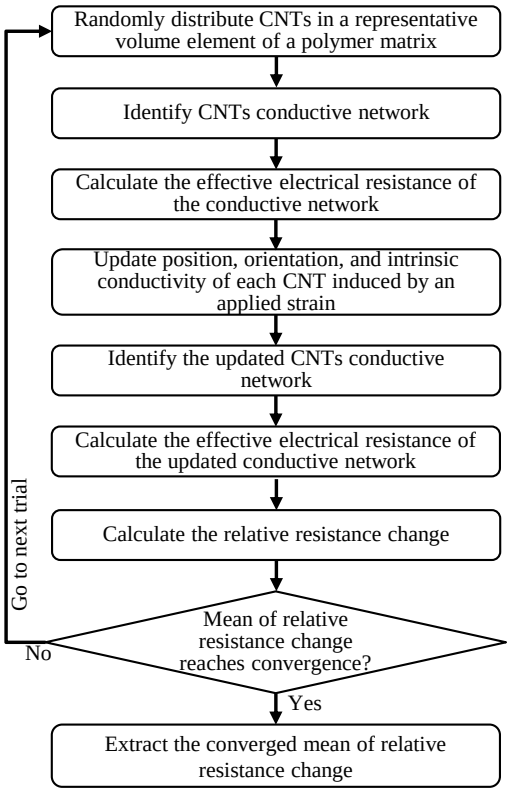

Figure 4.1 An overview of the Monte Carlo simulation procedures

4.1.1 Transformation of the CNT network in a PNC under applied strain

The transformation of the embedded CNTs (i.e., translation and rotation) caused by external mechanical strain is related to the deformation of CNT doped polymer matrix whose Poisson's ratio is chosen to be 0.35 (Fernberg 2009). It can be determined based on an affine transformation (Taya 1998). The translation of the center-point of the i^{th} CNT is determined by Equations (4.1a) through (4.1c).

$$x'_{c,i} = x_{c,i}(1+\varepsilon_{ploy}) \tag{4.1a}$$

$$y'_{c,i} = y_{c,i}(1-\upsilon\cdot\varepsilon_{poly}) \tag{4.1b}$$

$$z'_{c,i} = z_{c,i}(1-\upsilon\cdot\varepsilon_{poly}) \tag{4.1c}$$

where ($x_{c,i}$, $y_{c,i}$, $z_{c,i}$) and ($x'_{c,i}$, $y'_{c,i}$, $z'_{c,i}$) are the coordinates of the center-point of the i^{th} CNT with and without strain; ε_{poly} is the applied strain on the PNC; and υ is the PNC's Poisson's ratio.

Using φ_i and θ_i, the relationships between (ε_{poly}, υ) and (φ'_i,θ'_i) can be expressed as in Equations (4.2a) through (4.2c).

$$1+\varepsilon_{poly} = \frac{L'_{CNT,x}}{L_{CNT,x}} = \frac{L_{CNT}\cos\theta'_i}{L_{CNT}\cos\theta_i} \tag{4.2a}$$

$$1-\upsilon\cdot\varepsilon_{poly} = \frac{L'_{CNT,y}}{L_{CNT,y}} = \frac{L_{CNT}\cos\varphi'_i\sin\theta'_i}{L_{CNT}\cos\varphi_i\sin\theta_i} \tag{4.2b}$$

$$1-\upsilon\cdot\varepsilon_{poly} = \frac{L'_{CNT,z}}{L_{CNT,z}} = \frac{L_{CNT}\sin\varphi'_i\sin\theta'_i}{L_{CNT}\sin\varphi_i\sin\theta_i} \tag{4.2c}$$

Then, the updated (φ'_i, θ'_i) are determined by Equations (4.3a) and (4.3b).

$$\varphi'_i = \varphi_i \tag{4.3a}$$

$$\tan\theta'_i = \frac{1-\upsilon\cdot\varepsilon_{poly}}{1+\varepsilon_{poly}}\tan\theta_i \tag{4.3b}$$

Using the updated coordinates of the CNTs, the reconfigured CNT network under applied strain (i.e., ε_{poly}) can be identified. Moreover, the strain of individual CNT is linearly proportional to ε_{poly} (Hu 2012). The strain-induced change in the intrinsic conductivity (i.e., σ_{CNT}) of the i^{th} CNT can be updated by Equation (4.4).

$$\sigma'_{CNT_i} = \frac{\sigma_{CNT}}{1+2.118\cdot\alpha\cdot\varepsilon_{poly}\cdot\cos^2\theta'_i} \tag{4.4}$$

where 2.118 is the estimated CNTs' piezoresistivity calculated by Hu *et al.* (Hu 2012); and α is the strain ratio of CNT to polymer.

The value of σ'_{CNT} is obtained for each individual CNT due to the difference in the polar angle (i.e., θ_i). The revised $R_{intrinsic}$ can be calculated by Equations (3.4) and (4.4). Furthermore, upon the transformation of the CNTs in the conductive network, it is necessary to revise $R_{contact}$ by using Equations (3.5a) through (3.5c) and the updated coordinates of the two interconnecting CNTs. The new PNC's effective resistance (R'), under ε_{poly}, can then be determined. The relative change of the strain-induced resistance ($\Delta R/R$) can subsequently be calculated by Equation (4.5).

$$\frac{\Delta R}{R} = \frac{R' - R}{R} \tag{4.5}$$

where ΔR is the change in the PNC's resistance; and R' are the resistances after applying strain.

4.1.2 Mechanisms contributed to the piezoresistivity of PNCs filled with CNTs

PNC's piezoresistivity can be attributed to strain-induced reconfiguration of embedded CNT network, which consists of many independent conductive paths. When strain is applied to PNCs, it will induce morphological changes to these conductive paths. We propose that the potential morphological changes can be classified into three mechanisms as shown in Figures 4.2.

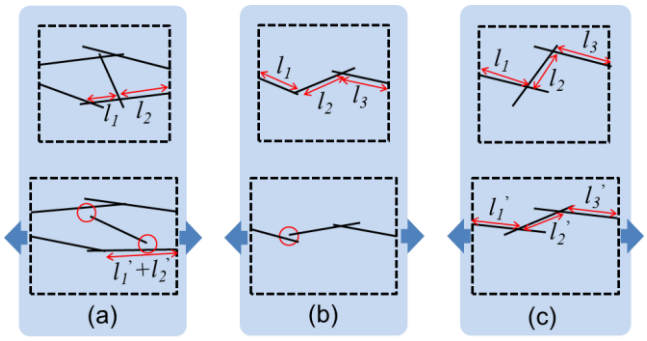

Figure 4.2 Mechanisms of strain-induced PNC's morphological change: (a) breakage of a complex conductive path into two or more simpler paths (Type I); (b) breakage of a conductive path (Type II); and (c) alternation of a conductive path without breakage (Type III)

Under Type I mechanism, illustrated in Figure 4.2(a), a complex conductive network comprises of many CNTs is broken down into several simpler networks. This is caused by disconnecting individual CNTs from the network due to their translation and reorientation. Consequently, the equivalent resistance of the conductive network will moderately increase. Under Type II mechanism, illustrated in Figure 4.2(B), the translation and reorientation of individual CNTs along a conductive path will break because of the separation of CNTs at their junctions beyond a threshold (Kirkpatrick 1973). As the conductive pathway has been disrupted, it would lead to a more significant reduction in the conductive network's equivalent resistance than Type I mechanism. Under Type III mechanism, illustrated in Figure 4.2(c), the separation distance between two CNTs at a junction increases slightly. This will result in a minor decrease in the equivalent resistance of the CNT conductive network. Under all three mechanisms, the intrinsic piezoresistivity of CNTs will also contribute to the macroscopic piezoresistivity of the PNC (Hu 2012).

In order to systematically analyze the contributions of each proposed mechanism to PNC's piezoresistivity, a set of parameters related to the morphological changes are defined and their relationships to PNCs' piezoresistivity are summarized in Table 4.1. Moreover, to identify the contribution of the three proposed mechanisms on the piezoresistivity of PNCs, the changes in the five key morphological parameters under each mechanism are indicated in Table 4.2.

Table 4.1 Morphological parameters related to PNCs' piezoresistivity

Morphological Parameters	**Relationships to the Conductive Network**
Total number of CNTs in the conductive network (N_{CNT})	Represents the number density of CNTs in the conductive network
Total number of independent conductive paths in the CNT network (N_{path})	Represents the degree of percolation
Average polar angle of CNTs (θ_{avg})	Represents the degree of CNT alignment
Average junction-to-junction distance along a CNT in conductive paths (l_{avg})	Influences average value of intrinsic resistances in the conductive network
Average CNT-to-CNT distance at junctions (d_{avg})	Influences average value of tunneling resistances in the conductive network

Table 4.2 Changes in morphological parameters under the three types of mechanisms

Mechanism	N_{CNT}	N_{path}	θ_{avg}	l_{avg}	d_{avg}
Type I	↓	↑↑↑	↓↓↓	↑↑↑	-
Type II	↓↓↓	↓↓↓	↓↓↓	↓↓↓	-
Type III	-	-	↓↓↓	-	-
↑↑↑ strong positive effect; ↑ weak positive effect; ↓↓↓ strong negative effect; ↓ weak negative effect; - negligible effect					

Applying external strain to the PNCs would induce rotational motion on the embedded CNTs. Therefore, the CNTs would be more aligned in the stretching direction, and would reduce θ_{avg}. Under Type I mechanism, a small number of CNTs that bridge multiple conductive paths are disconnected from the network. Therefore, it would have a small negative effect on N_{CNT} while a strong positive effect on N_{path}. As the corresponding junctions are removed, Type I mechanism would increase l_{avg}. Under Type II mechanism, some existing

CNT conductive paths are disrupted. Hence, it would significantly reduce both N_{CNT} and N_{path}. Moreover, since the simple CNT conductive paths associated with Type II mechanism usually have long junction-to-junction distances, their removal from the network would have a strong negative impact on l_{avg}. Type III mechanism only involves rotation and translation of CNTs without removing them from the conductive network. Thus, it has negligible effect on all the morphological parameters except θ_{avg}. However, upon continuous increase in strain, Type III mechanism would eventually be transformed into Type II mechanism, resulting in dramatic effects on PNC's piezoresistivity.

4.2 Results and discussion

Using the described theoretical framework, the relative changes of PNCs' resistances under different levels of strain were determined. As the discussion in Chapter 3, the dimensions of RVEs were set to $4 \times L_{CNT}$ by $1.1 \times L_{CNT}$ by $1.1 \times L_{CNT}$. Simulation results were compared with experimental data (Park 2008, Fernberg 2009) for PNCs loaded with either different contents or different grades of CNTs to verify the model. After the validation, systematic studies were conducted to quantitatively analyze the impacts of different proposed mechanisms on PNCs' piezoresistivity.

4.2.1 Validation of the 3D model and the simulation scheme

The predicted piezoresistivity of PNCs filled with multi-walled carbon nanotubes (MWNTs) were compared with experimental data of MWNT/PEO PNCs reported by Park *et al.*(Park 2008). The experimental measurements were extracted from the plot of resistance

change (i.e., $\Delta R/R$) versus strain (i.e., ε_{poly}). Following the parameters described in their study, L_{CNT} and D were set to be 2.5 μm and 15 nm, respectively, in the simulation. σ_{CNT} was determined to be 1100 S/m (Naeemi 2009). Figure 4.3(a) compares the simulated piezoresistive behaviours and the experimental data of PNCs loaded with 0.56 *vol.*% and 1.44 *vol.*% MWNTs. It can be observed that the simulation results agreed with the experimental data at both MWNT loadings. In order to further confirm the validity of the model and simulation scheme, the piezoresistivity of MWNT-doped epoxy filled with 0.5 *wt.*% of MWNT reported by Fernberg *et al.* (Fernberg 2009) was also simulated. The experimental results of PNCs' piezoresistivity were converted from the plot of different resistivity of specimen at varying strain. L_{CNT} and D were set to be 5 μm and 15 nm, respectively, according to the MWNT's characteristics in their work. σ_{CNT} were determined to be 2100 S/m (Naeemi 2009). As shown in Figure 4.3(b), a good agreement between the simulation result and the experimental data had been achieved for the MWNT-doped epoxy's piezoresistivity. Overall, it demonstrated that the proposed model and simulation scheme can be used as realistic tools to quantitatively analyze the piezoresistive behaviours of PNCs.

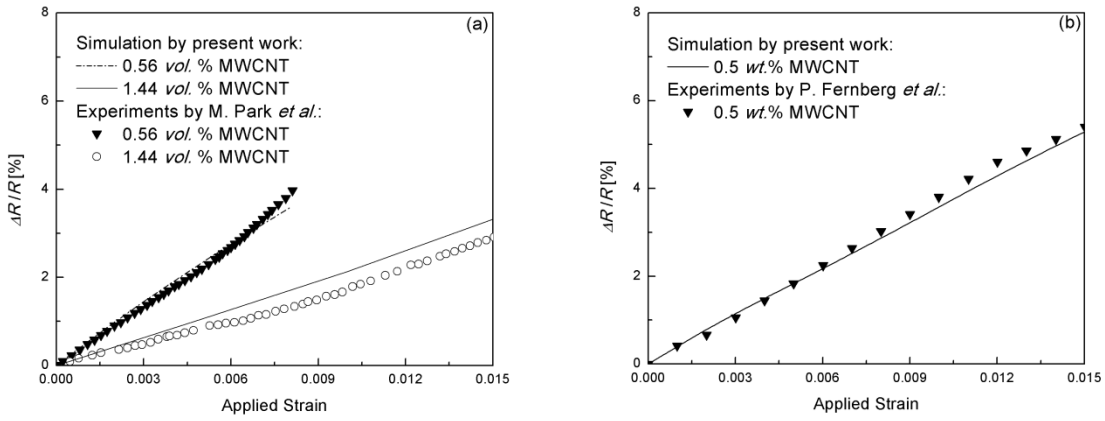

Figure 4.3 Comparison of simulation results of PNCs' piezoresistivity with existing experimental data reported by (a) Park et al. and (b) Fernberg et al.

4.2.2 Key governing factors to PNCs' piezoresistivity

The underlying mechanisms for PNCs' piezoresistivity were investigated by quantitatively analyzing different strain-induced morphological changes. These included the relative changes in (i) total number of CNTs in the conductive network (N_{CNT}), (ii) average polar angle (θ_{avg}) of CNTs, (iii) average intrinsic resistance along a CNT between two junctions ($R_{intrinsic,avg}$), and (iv) average tunneling resistance at CNT junctions ($R_{contact,avg}$). MWNT/PEO PNCs loaded with 0.56 and 0.80 *vol.*% of MWNTs were considered herein as case examples.

Figure 4.4(a) and (b) plot the strain-induced relative changes of these parameters for PNCs loaded with different MWNT contents. The relative change of N_{CNT} for the PNC loaded with 0.56 *vol.*% MWNT had a more negative slope than that loaded with 0.80 *vol.*% MWNT, while the slopes of the relative changes of θ_{avg}, $R_{intrinsic,avg}$, and $R_{contact,avg}$ were similar at both

MWNT loadings. The negligible change in $R_{contact,avg}$ suggested an insignificant influence of strain on $R_{contact}$ at MWNT-to-MWNT junctions. Moreover, N_{CNT} and θ_{avg} decreased linearly while $R_{intrinsic,avg}$ increased linearly with increased strain. The elongation of PNCs led to rotational and translational motions for all MWNTs. The rotational motion tended to promote the alignment of MWNTs along the straining direction, leading to a decrease in θ_{avg}. The reduction in N_{CNT} could be attributed to both Type I and Type II mechanisms. MWNT's rotation and translation would cause some MWNTs that bridged multiple conductive paths disconnected from the conductive network. This broke some of the complex MWNT network into simpler ones (i.e., Type I mechanism) and reduced N_{CNT}. Strain could also induce breakage of some junctions along simpler conductive paths (i.e., Type II mechanism) and further decreased N_{CNT}.

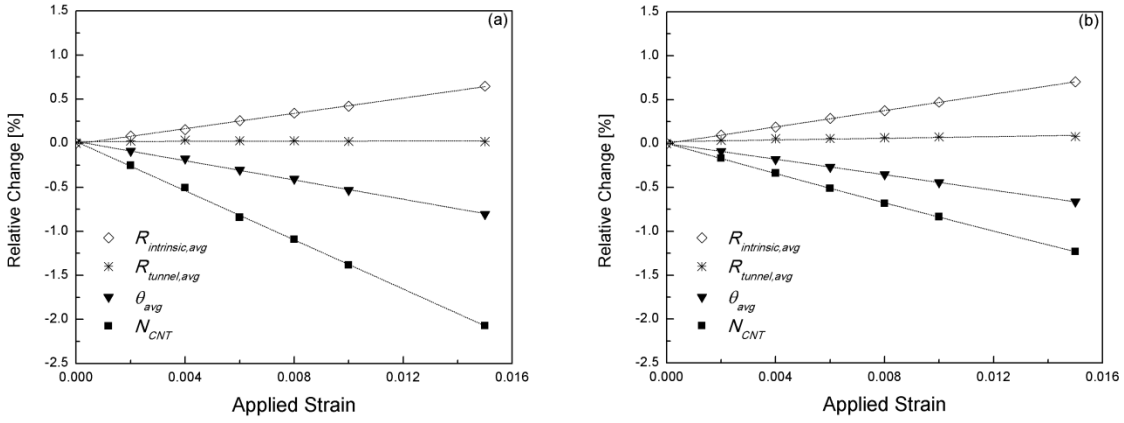

Figure 4.4 Strain-induced relative changes in quantifiable parameters at (a) 0.56 and (b) 0.80 *vol.*% of MWNTs.

The drop in $R_{intrinsic,avg}$ could potentially be attributed to two factors: (i) intrinsic piezoresistivity of an individual MWNT, and (ii) change in distance between adjacent

junctions along an individual MWNT. Consistent with the work reported by Hu *et al.* (Hu 2012), the strain-induced change in σ_{CNT} had limited influence on the PNCs' macroscopic piezoresistive behaviours. Under Type I mechanism, the separation of MWNTs from the conductive network would remove some MWNT-to-MWNT junctions. This would in turn increase the distance between adjacent junctions along a MWNT, leading to the change in $R_{intrinsic,avg}$.

4.2.3 Effects of CNT loadings on PNCs' piezoresistive behaviours

PNCs' macroscopic piezoresistivity was shown to be predominantly affected by changes in the conductive network's morphology. Thus, the relative changes in the five morphological parameters summarized in Table 4.2 were simulated. Figures 4.5(a) and (b) depict the results for PNCs loaded with 0.56 and 0.80 *vol.*% MWNTs subjected to strain. In both cases, larger strain would increase N_{path} and l_{avg} while decrease N_{CNT} and θ_{avg}. However, strain had negligible effect on d_{avg}.

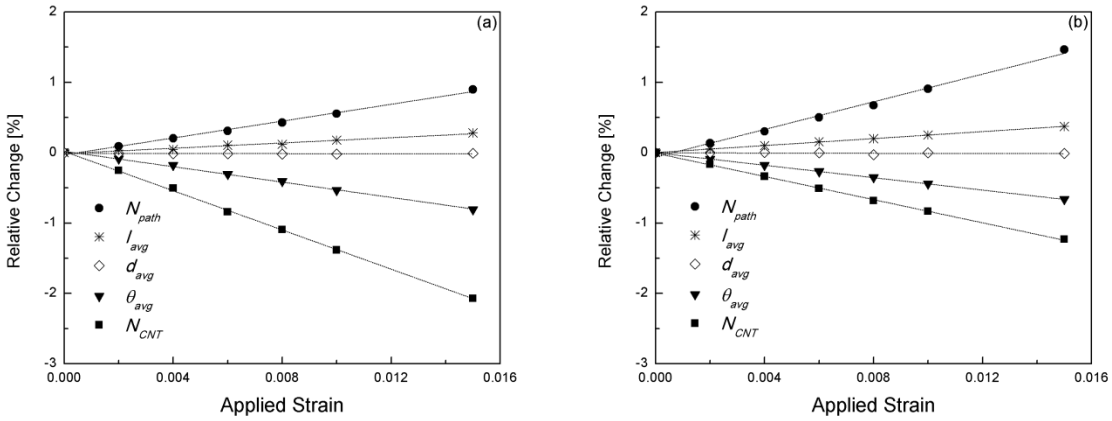

Figure 4.5 Strain-induced relative changes in different morphological parameters of the conductive network at (a) 0.56 and (b) 0.80 *vol.*% of MWNTs.

While both Type I and Type II mechanisms would contribute to the piezoresistivity, the decrease in N_{CNT} together with the hike in both N_{path} and l_{avg} suggested that Type I mechanism had a larger contribution than Type II mechanism. It was also found that higher MWNT loadings would increase the complexity of conductive paths. Simulation results suggested that each conductive path consists of an average of 46 MWNTs in PNCs with 0.56 *vol.*% MWNT and 151 MWNTs in those with 0.80 *vol.*% MWNT. Therefore, increasing MWNT loadings would promote the contribution of Type I mechanism to the PNC's piezoresistivity while suppress that of Type II mechanism. As Type I mechanism only partially disrupts the network while Type II mechanism completely breaks a conductive pathway, the enhancement to Type I mechanism would reduce PNC's piezoresistivity. In addition, Figures 4.5(a) and (b) show that PNCs filled with higher MWNT loading lessened the relative decrease in N_{CNT} while surged the relative increase in N_{path}. Hence, the dominance of Type I mechanism to the piezoresistivity increased with CNT loadings. Although Type III mechanism should also exist, its influence on the PNCs' piezoresistivity was minimal until larger strain shifted it to Type II mechanism.

4.2.4 Effects of CNT alignment on PNCs' piezoresistivity

The effects of CNT alignment on PNCs' piezoresistivity were simulated by varying the maximum polar angle between the i^{th} CNT and the x-axis (i.e., θ_{max}). Figures 4.6(a) and (b) show that the effects of θ_{max} on the electrical conductivity (σ_{PNC}) and piezoresistivity of PNCs with different MWNT loadings. A small θ_{max} (e.g., 35°) meant that MWNTs were preferentially aligned while a large θ_{max} (e.g., 90°) meant that MWNTs were more randomly oriented. For both MWNT loadings, σ_{PNC} increased rapidly when reducing the degree of CNT alignment at

small θ_{max}. It then reached a plateau as θ_{max} increased, and eventually dropped slightly as θ_{max} approached 90°. In other words, there existed an optimal θ_{max} to promote σ_{PNC}. Consistent with the previous discussion in section 3.2.4 and the literature (Bao 2011, Du 2005), Figures 4.5(a) illustrates that the optimal θ_{max} was larger for PNCs with lower MWNT loadings. Du *et al.* (Du 2005) discovered that the filler start to form a conductive network at a critical point upon increasing the isotropy (i.e., decreasing the alignment). This produces a dramatic increase in electrical conductivity (e.g., the significant increment in Figures 4.5(a)). Similar to the percolation threshold theory, such alignment threshold (i.e., $\theta_{max,c}$) can be evaluated using power law fitting as expressed in Equation (4.6).

$$\sigma = \sigma_0(\theta_{max} - \theta_{max,c})^t \text{ for } \theta_{max} > \theta_{max,c} \tag{4.6}$$

where σ_0 is a parameter attributed to the intrinsic conductivity of CNTs; and t is the critical exponent, which is known to be dominated by the dimensionality of the system (Kirkpatrick 1973).

The $\theta_{max,c}$ were calculated to be 25° and 35° for PNCs loaded with 0.56 and 0.80 *vol.*% MWNTs, respectively. Figures 4.6(a) and (b), revealed that increasing filler alignment would significantly reduce σ_{PNC} near the alignment threshold, while dramatically promote PNCs' piezoresistivity. Thus, higher degree of CNT alignment near $\theta_{max,c}$ would enhance PNCs' piezoresistivity. This could be attributed to the simple and fragile conductive networks formed by highly-aligned MWNTs. This finding agreed with the experimental studies conducted by Oliva-Avilés *et al.* (Oliva-Avilés 2011). Their study revealed that higher

piezoresistivity was obtained for MWNT/PSF films with pre-aligned MWNTs induced by an AC electric field.

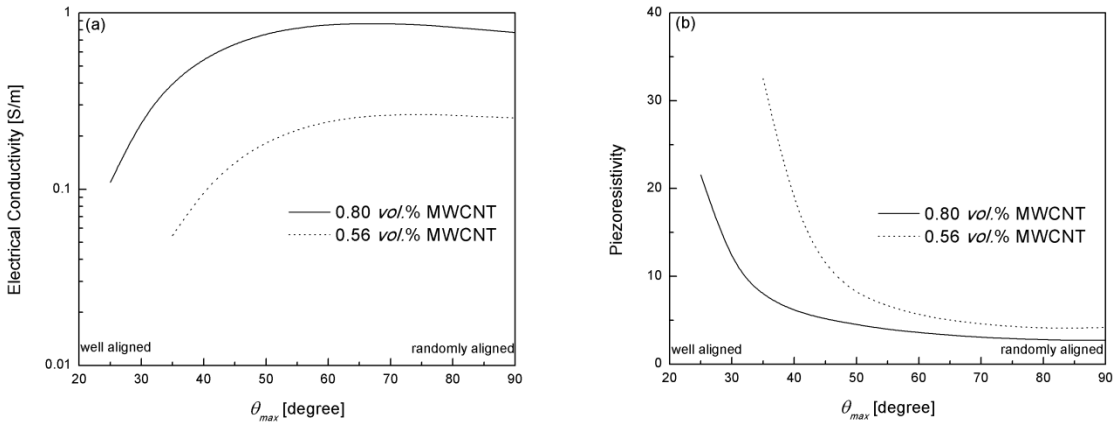

Figures 4.6 Effects of CNT alignment on (a) Electrical conductivity and (b) piezoresistivity of PNCs at 0.56 and 0.80 *vol.*% of MWNTs.

Strain was shown to have negligible influence on d_{avg} and consistent effect on θ_{avg} (i.e., decrease). Thus, our simulations to study the effects of CNT alignment on PNC's piezoresistivity focused on l_{avg}, N_{path}, and N_{CNT}. Figures 4.7(a) through (c) show the effects of CNT alignment on the relative changes in these parameters when PNCs loaded with 0.56 *vol.*% MWNT were strained. It can be observed that higher degrees of MWNT alignment would reduce the strain-induced increases in l_{avg} and N_{path}, while promote the decrease in N_{CNT}. Figure 4.7(d) shows the rate of relative changes in these parameters with respect to the applied strain (i.e., the slopes of the linear lines in Figures 4.7(a) through (c)). Most importantly, the rate of relative change in l_{avg} changed from negative to positive at θ_{max} equaled to approximately 40° as θ_{max} increased. This suggests that Type II mechanism for PNC's piezoresistivity would be more pronounced for PNCs embedded with highly aligned

CNTs, while Type I mechanism for PNC's piezoresistivity would take over when CNTs became more randomly oriented. Moreover, the average numbers of MWNTs per conductive path were determined to be 7 and 46 for θ_{max} equaled to 35° and 90°, respectively. In other words, high degree of CNT alignment would promote the formation of simple CNT network, leading to the increase significance of Type II mechanism.

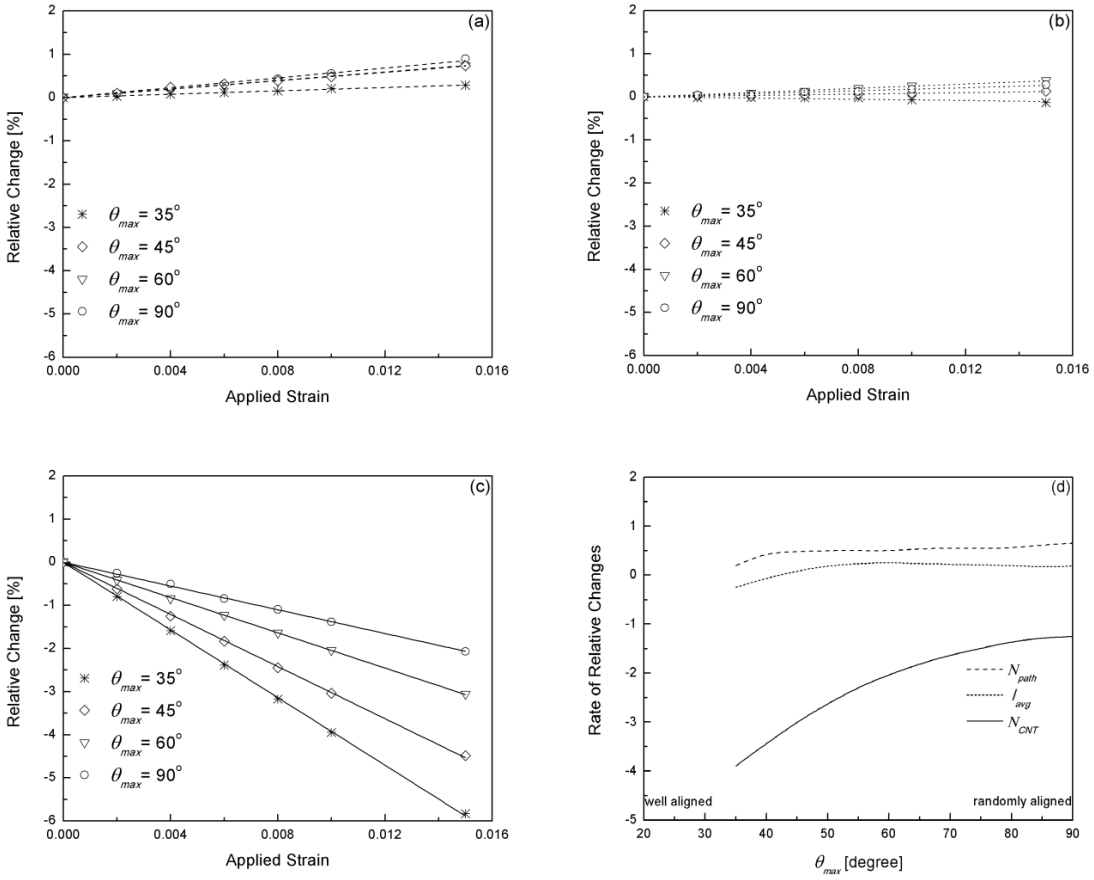

Figures 4.7 Effects of CNT alignment on the relative changes of (a) N_{path}, (b) l_{avg}, (c) N_{CNT}, and (d) rate of relative changes in these parameters, at 0.56 *vol.*% MWNTs loading.

The effects of CNT alignment on the relative changes in l_{avg}, N_{path}, and N_{CNT} when straining PNCs with 0.80 *vol.*% MWNTs are illustrated in Figures 4.8(a) through (c). Similar

to the trends for PNCs with lower MWNT loading, preferential MWNT alignment would reduce the strain-induced increases of l_{avg} and N_{path}, but promote the decrease in N_{CNT}. Moreover, Figure 4.8(d) reveals that the rate of relative change in l_{avg} remained positive at all θ_{max} from 25° to 90°, suggesting that the higher MWNT loading led to the predominance of Type I mechanism for PNC's piezoresistivity, even for the cases of PNCs with high degree of MWNT alignment. This can be attributed to the increased complexity of CNT network with higher MWNT loadings.

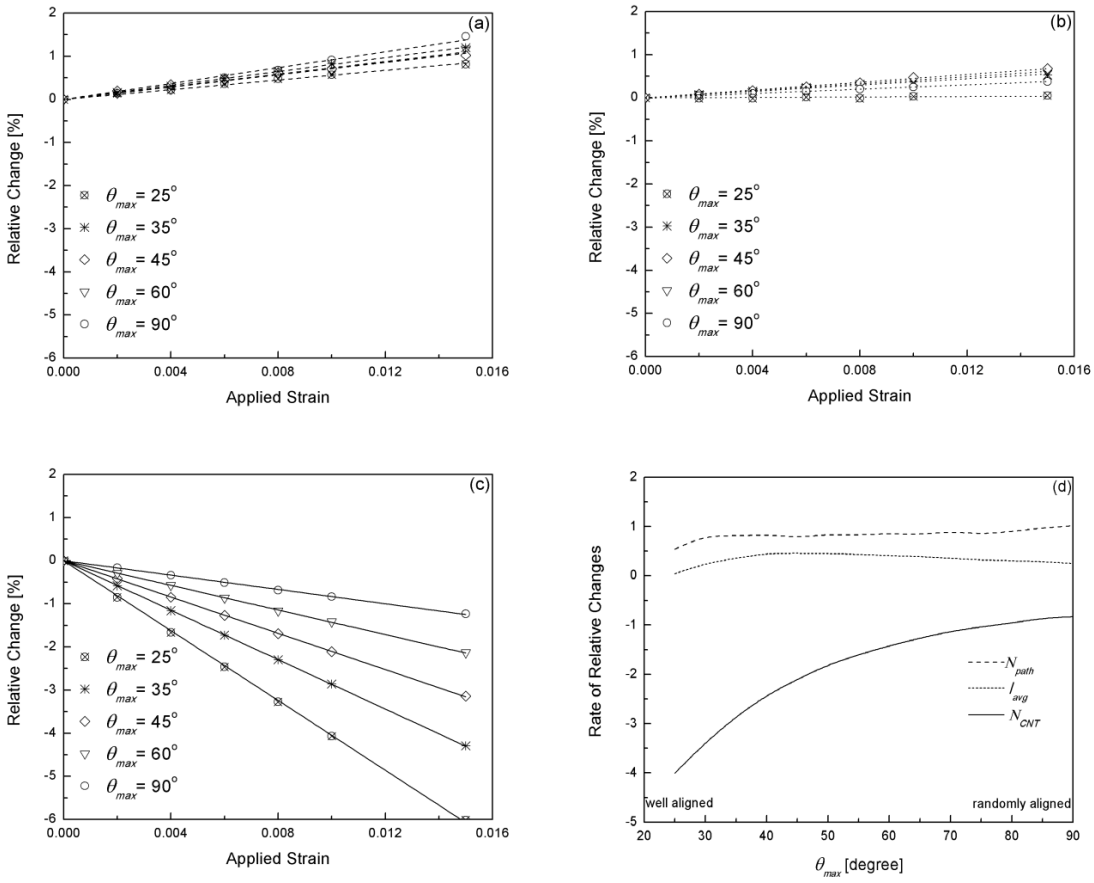

Figure 4.8 Effects of CNT alignment on the relative changes of (a) N_{path}, (b) l_{avg}, (c) N_{CNT}, and (d) rate of relative changes in these parameters, at 0.80 *vol.*% MWNTs loading.

4.3 Concluding Remarks

This work extends an advanced 3D resistor network model to simulate PNCs' piezoresistive responses to external strain. The model and the simulation scheme were verified by comparing the simulation results with experimental data of PNC's piezoresistivity. Three mechanisms contributed to piezoresistivity have been proposed in this paper. These mechanisms include: (Type I) breakage of a complex conductive network into two or more simpler conductive paths; (Type II) disruption of a conductive path; and (Type III) alternation of a conductive path without breakage. Among them, Type II mechanism would lead to higher piezoresistivity when comparing to Type I mechanism because of the complete breakage of conductive paths. While Type III mechanism has negligible direct impact on the piezoresistive behaviours of PNCs, it is the precursor of Type II mechanism. Quantitative analyses on strain-induced changes in different morphological parameters revealed different structures of PNCs (e.g., CNT contents or CNT alignment) would favor different mechanisms for PNC's piezoresistivity. For PNCs filled with randomly dispersed CNTs, Type I mechanism predominantly contributed to the PNC's piezoresistivity while Type II mechanism's influence was less significance. Moreover, the dominance of Type I mechanism was more pronounced for PNCs with higher CNT loadings, because of the increased complexity of CNT network. On the other hand, preferential CNT alignment would also affect the dependence of PNC's piezoresistivity on different mechanisms. For PNCs filled with low content of highly aligned CNTs, the PNCs' piezoresistivity was mainly caused by Type II mechanism due to the small number of CNTs in each conductive path. The contribution of Type I mechanism became more pronounced as CNT loading increased. The

identified underlying mechanisms for PNC's piezoresistivity and their relationships to PNC's morphology provide insights to optimize the micro-and-nanostructures of PNCs, which would help enhancing the sensitivity of these smart materials for strain sensing applications.

CHAPTER 5 Concluding Remarks

5.1 Summary of Conclusions

This thesis developed a realistic and efficient modeling framework to describe the three dimensional carbon nanotube networks in polymer nanocomposites. The newly developed novel model was applied to reveal the electrical conductivity of carbon nanotube based polymer nanocomposites. The following conclusions have been promoted through this thesis:

1. In the three dimensional modeling of carbon nanotube networks in polymer nanocomposites, the contribution of interconnecting carbon nanotubes across the boundary surfaces of the representative volume element should been accounted, in order to avoid unnecessary biases in the spatial dispersion and length distribution of carbon nanotubes being caused by the "cut-and-relocate" approach adopted in typical models found in literatures. The size of the representative volume element can be decreased, and thereby significantly reduce the computational cost of the Monte Carlo simulations

2. Using the newly developed model to simulate the electrical conductivity of carbon nanotube based polymer nanocomposites, it has revealed that the electrical conductivity is only influenced by the dimension of representative volume element in parallel to the direction of the current flow. The length in dimensions perpendicular to the direction of the current flow can be significantly reduced without affecting the simulation results.

3. A series of Monte Carlo simulations, using the newly developed novel model, were conducted to simulate the electrical conductivity of polymer nanocomposites based on different grades of multi-walled carbon nanotubes. The simulation results agreed with those reported in existing experimental studies. It was demonstrated that the novel model developed in this thesis significantly increase the efficiency of the Monte Carlo simulations while maintaining the results accuracy.

4. This novel model was applied to the numerical study on the effects of carbon nanotube's orientation on electrical conductivity of polymer nanocomposites. It has been revealed that randomly orientated carbon nanotubes leads to lower percolation threshold, while highly aligned carbon nanotubes along the direction of electric current lead to higher electrical conductivity at high carbon nanotube loadings.

Furthermore, this thesis extended the newly developed novel model of three dimensional carbon nanotube networks to expose the governing mechanisms of the carbon nanotube based polymer nanocomposites' piezoresistivity. The following conclusions have been promoted:

1. Three governing mechanisms contributing to the piezoresistivity of carbon nanotube based polymer nanocomposites are proposed in this thesis study, namely (Type I) breakage of a complex conductive network into two or more simpler conductive paths; (Type II) disruption of a conductive path; and (Type III) alternation of a conductive path without breakage.

2. Among these governing mechanisms, Type II mechanism would lead to higher piezoresistivity of carbon nanotube based polymer nanocomposites when comparing to Type I mechanism because of the complete breakage of conductive paths. Though, Type III mechanism has negligible direct impact on the piezoresistive behaviours, it is the precursor of Type II mechanism. Quantitative analyses on strain-induced changes in different morphological parameters revealed that different structures of carbon nanotube based polymer nanocomposites (e.g., carbon nanotube contents or alignment) would favor different types of the mechanisms for PNC's piezoresistivity.

3. For PNCs filled with randomly dispersed carbon nanotube, Type I mechanism predominantly contributed to the piezoresistivity of carbon nanotube based polymer nanocomposites, while Type II mechanism's influence was less significance. Moreover, the dominance of Type I mechanism was more pronounced for polymer nanocomposites with higher carbon nanotube contents, because of the increased complexity of the electrically conductive network.

4. Along with carbon nanotube contents, preferential CNT alignment would affect the dependence of polymer nanocomposites' piezoresistivity on different types of the mechanisms. For polymer nanocomposites filled with highly aligned carbon nanotubes, the contribution of Type II mechanism were enhanced due to the simplicity of the each electrically conductive path (i.e., small number of carbon nanotubes in the path).

5.2 Summary of Contributions

The significant research contributions presented in this thesis are summarized as follows:

1. The novel model newly developed in this thesis work significantly reduced the computational cost of the Monte Carlo simulation without compromising the accuracy. It would serve as a realistic strategic design tool to fabricate carbon nanotube based polymer nanocomposites with tailored electrical conductivity by controlling carbon nanotube loading and orientation.

2. The identified underlying mechanisms for the piezoresistivity of carbon nanotube based polymer nanocomposites and their relationships to the morphology of conductive network with nanocomposites provided the enormous insights to optimize the micro-and-nanostructures of carbon nanotube based polymer nanocomposites, which would help enhancing the sensitivity of these smart materials for strain sensing applications.

5.3 Scholarly Publications

The research work presented in this thesis has been disseminated via two refereed journal publications, two conference publications and presentations detailed as follows:

Refereed journal publications

1. Fang, W., and Leung, S.N., "Elucidation of Structure-to-Property Relationships of Piezoresistive Polymer-Carbon Nanotube Nanocomposites," Journal of Applied Physics, Vol. 118, Issue 4, pp. 044907, 2015.

2. Fang, W., Jang, H.W., and Leung, S.N., "Evaluation and Modelling of Electrically Conductive Polymer Nanocomposites with Carbon Nanotube Networks," Composites Part B: Engineering, Vol. 83, pp. 184-193, 2015.

Conference publications and presentations

1. Fang, W., Leung, S.N., and Zhu, Z.H., "Electrical Conductivity Modeling of Carbon Nanotube Networks in Polymer Nanocomposites and Their Foams," CSME International Congress, Toronto, ON, Canada, June 1-4, 2014.

2. Fang, W. and Leung, S.N., "Impacts of Different Mechanisms on Carbon Nanotubes/Polymer Nanocomposites' Piezoresistivity," SPE, ANTEC, Technical Papers, Paper #2086485, Orlando, FL, USA, March 23-25, 2015.

List of References

Akima, N., Iwasa, Y., Bron, S., Barbour, A. M., Cao, J., Musfeldt, J. L., Matsui, H., Toyota, N., Shiraishi, M., Shimoda, H., and Zhou, O. (2006). Strong anisotropy in the far-infrared absorption spectra of stretch-aligned single-walled carbon nanotubes. *Advanced Materials*, 18, 1166-1169.

Alamusi, Hu, N., Fukunaga, H., Atobe, S., Liu, Y., and Li, J. (2011). Piezoresistive strain sensors made from carbon nanotubes based polymer nanocomposites. *Sensor*, 11, 10691.

Bao, W. S., Meguid, S. A., Zhu, Z. H., and Meguid, M. J. (2011). Modeling electrical conductivities of nanocomposites with aligned carbon nanotubes. *Nanotechnology*, 22, 485704.

Bao, W. S., Meguid, S. A., Zhu, Z. H., and Weng, G. J. (2012). Tunneling resistance and its effect on the electrical conductivity of carbon nanotube nanocomposites. *Journal of Applied Physics*, 111, 093726.

Behnam, A., Guo, J. and Ural, A. (2007). Effects of nanotube alignment and measurement direction on percolation resistivity in single-walled carbon nanotube films. *Journal of Applied Physics*, 102, 044313.

Buldum, A., and Lu, J. P. (2001). Contact resistance between carbon nanotubes. *Physical Review B*, 63, 161403-161406.

Dalton, A. B., Collins, S., Moñoz, E., Razal, J. M., Ebron, V. H., Ferraris, J. P., Coleman, J. N., Kim, B. G., and Baughman, R. H. (2003). Super-tough carbon-nanotube fibres. *Nature*, 423, 703.

Davies, D. K. (1969). Charge generation on dielectric surface. *Journal of Physics D: Applied Physics*, 2, 1533-1537.

Du, F., Fischer, J. E., and Winey, K. I. (2005). Effect of nanotube alignment on percolation conductivity in carbon nanotube/polymer composites. *Physical Review B: Condensed Matter and Material Physics*, 72, 121404.

Ebbesen, T. W., Lezec, H. J., Hiura, H., Bennet, J. W., Ghaemi, H. F., and Thio, T. (1996). Electrcal conductivity of individual carbon nanotube. *Nature*, 82, 54-56.

Fernberg, P., Nilsson, G., and Joffe, R. (2009). Piezoresistive performance of long-fiber composites with carbon nanotube doped matrix. *Journal of Intelligent Material Systems and Structures*, 20, 1017.

Girifalco, L. A., Hodak, M., and Lee, R. S. (2000). Carbon nanotubes, buckyballs, ropes, anda universal graphitic potential. *Physical Review B*, 62, 13104.

Girifalco, L. A., Hodak, M., and Lee, R. S. (2000). Carbon nanotubes, buckyballs, ropes, anda universal graphitic potential. *Physical Review B*, 62, 13104.

Glenis, S., Likodimos, V., Guskos, N., Yarmis, D., Zolnierkiewicz, G., Szymczyk, A., and Lin, C. L. (2010). Magnetic properties of carbon nanotube poly(ether-ester) nanocomposites. *Journal of Applied Physics*, 108, 054314.

Grujicic, M., Cao, G., and Roy, W. N. (2004). A computational analysis of the percolation threshold and the electrical conductivity of carbon nanotubes filled polymeric materials. *Journal of Materials Science*, 39, 4441-4449.

Hertel, T., Walkup, R. E., and Avouris, P. (1998). Deformation of carbon nanotubes by surface van der Waals forces. *Physical Review B*, 58, 13870-13873.

Hertel, T., Walkup, R. E., and Avouris, P. (1998). Deformation of carbon nanotubes by surface van der Waals forces. *Physical Review B*, 58, 13870-13873.

Hou, J., Wang, X., Vellelacheruvu, P., Guo, J., Liu, C., and Cheng, H. (2006). Thermal characterization of single-wall carbon nanotube bundles using the self-heating 3ω technique. *Journal of Applied Physics*, 100, 124314.

Hu, G., Zhao, C., Zhang, S., Yang, M., and Wang, Z. (2006). Low percolation thresholds of electrical conductivity and rheology in poly(ethylene terephthalate) through the networks of multi-walled carbon nanotubes. *Polymer*, 47, 480-488.

Hu, N., Masuda, Z., Yan, C. Y., Yamamoto, G., Fukunaga, H., and Hashida, T. (2008**a**). The electrical properties of polymer nanocomposites with carbon nanotube fillers.

Nanotechnology, 19, 215701.

Hu., N., Karube, Y., Yan, C., Masuda, Z., and Fukunaga, H. (2008b). Tunneling effect in a polymer/carbon nanotube nanocomposite strain sensor. *Acta Materialia*, 56, 2929-2936.

Kirkpatrick, S. (1973). Percolation and conduction. *Reviews of Modern Physics*, 45, 574.

Knudsen, H. A., and Fazekas, S. (2006). Robust algorithm for random resistor networks using hierarchical domain structure. *Journal of Computational Physics*, 211, 700-718.

Kukovecz, A., Kanyo, T., Konya, Z., and Kirisci, I. (2005). Long-time low-impact ball milling of multi-wall carbon nanotubes. *Carbon*, 43, 994-1000.

Kymakis, E., Alexandou, I., and Amaratunage, G. A. J. (2002). Single-walled carbon nanotube–polymer composites: electrical, optical and structural investigation. *Synthetic Metal*, 127, 59-62

Li, C., Thostenson, E. T., and Chou, T. W. (2007). Dominant role of tunneling resistance in the electrical conductivity of carbon nanotube–based composites. *Applied Physics Letters*, 91, 223114.

Li, H. J., Lu, W. G., Li, J. J., Bai, X. D., and Gu, C. Z. (2005). Multichannel ballistic transport in multiwall carbon nanotubes, *Physical Review Letters*, 95, 086601.

Marcus, M. S., Simmons, J. M., Castellini, O. M., Hamers, R. J., and Eriksson, M. A. (2006). Photogating carbon nanotube transistors. *Journal of Applied Physics*, 100, 084306.

Matsubara, E. Y., Rosolen, J. M., and Silva, S. R. P. (2008). Composite electrode of carbon nanotubes and vitreous carbon for electron field emission. *Journal of Applied Physics*, 104, 054303.

Moaseri, E., Karimi, M., Baniadam, M., and Maghrebi, M. (2014) Improvements in mechanical properties of multi-walled carbon nanotube-reinforced epoxy composites through novel magnetic-assisted method for alignment of carbon nanotubes. *Composites Part A: Applied Science and Manufacturing*, 64, 228-233.

Naeemi, A., and Meindl, J. D. (2009) Performance modeling for carbon nanotube interconnnects. In: Carbon nanotube electronics. New York: Springer, 163-190.

Nogales, A., Broza, G., Roslaniec, Z., Schulte, K., Sics, I., Hisao, B. S., Sanz, A., Garcia-Gutierrez, M. C., Rueda, D. R., Domingo, C., Ezquerra, T. A. (2004). Low percolation threshold in nanocomposites based on oxidized single wall carbon nanotubes and poly(butylene terephthalate). *Macromolucles*, 37, 7669-7872.

Oliva-Avilés, A. I., Avilés, F., and Sosa, V. (2011). Electrical and piezoresistive properties of multi-walled carbon nanotube/polymer composite films aligned by an electric field. *Carbon*, 49, 2989-2997.

Park, M., Kim, H., and Youngblood, J. P. (2008). Strain-dependent electrical resistance of multiwalled carbon nanotube/polymer composite films. *Nanotechnology*, 19, 055705.

Pham, G. T., Park, Y., Liang, Z., Zhang, C., and Wang, B. (2008). Processing and modeling of conductive thermoplastic/carbon nanotube films for strain sensing. *Composites Part B: Engineering*, 39, 209-2016.

Rubio, A., Sanchez-Portal, D., Aartacho, E., Ordejon, P., and Soler, J. M. (1999). Electronic states in a finite carbon nanotube: a one-dimensional quantum box. *Physical Review Letters*, 82, 3520.

Shiraishi, M., and Ata, M. (2001). Work function of carbon nanotubes. *Carbon*, 39, 1913-1917.

Shtogun, Y. V., and Woods, L. M. (2010). Mechanical properties of defective single wall carbon nanotubes. *Journal of Applied Physics*, 107, 061803.

Simmons, J. G. (1963). Generalized formula for the electric tunnel effect between similar electrodes separated by a thin insulating film. *Journal of Applied Physics*, 34, 1793-1803.

Taya, M., Kim, W. J., and Ono, K. (1998). Piezoresistivity of a short fiberrelastomer matrix composite. *Mechanics of Materials*, 28, 53-59.

Theodosiou, T. C., and Saravanos, D. A. (2010). Numerical investigation of mechanisms affecting the piezoresistive properties of CNT-doped polymers using multi-scale models.

Composites Science and Technology, 70, 1312-1320.

Venema, L. C., Wildoer, J. W. G., Janssen, J. W., Tans, S. J., Tuinstra, H. L. J., Kouwenhoven, L. P., and Dekker, D. (1999). Imaging electron wave functions of quantized energy levels in carbon nanotubes. *Science*, 283, 52-55.

Wang, S., Liang, Z., Wang, B., and Zhang, C. (2006). Statistical characterization of single-wall carbon nanotube length distribution. *Nanotechnology*, 17, 634-639.

Wang, X., Jiang, Q., Xu, W., Cai, W., Inoue, Y., and Zhu, Y. (2012). Effect of carbon nanotube length on thermal, electrical and mechanical properties of CNT/bismaleimide composites. *Carbon*, 53, 145-152.

Zamora-Ledezma, C., Blanc, C., and Anglaret, E. (2012). Controlled alignment of individual single-wall carbon nanotubes at high concentrations in polymer matrices. *Journal of physical Chemistry*, 116, 13760.

Zhou, W., Islam, M. F., Wang, H., Ho, D. L., Yodh, A. G., Winey, K. I., and Fischer, J. E. (2004). Small angle neutron scattering from single-wall carbon nanotube suspensions: evidence for isolated rigid rods and rod networks. *Chemical Physics Letters*, 384, 185-189.